UNIVERSITY OF OKLAHOMA

GRADUATE COLLEGE

DESIGN OF A NOVEL BIOREACTOR FOR ROTATOR CUFF TENDON TISSUE

ENGINEERING

A THESIS

SUBMITTED TO THE GRADUATE FACULTY

in partial fulfillment of the requirements for the

Degree of

MASTER OF SCIENCE

By

JIN LIU
Norman, Oklahoma
2018

DESIGN OF A NOVEL BIOREACTOR FOR ROTATOR CUFF TENDON TISSUE ENGINEERING

A THESIS APPROVED FOR THE
STEPHENSON SCHOOL OF BIOMEDICAL ENGINEERING

BY

_____
Dr. Matthias U. Nollert Chair

_____
Dr. Roger G. Harrison

_____
Dr. Vassilios I. Sikavitsas

Acknowledgements

love and support since the day I was born. I appreciate their continuous encouragement

throughout my years of study and through the process of researching and writing this

thesis. This accomplishment would not have been possible without them. Thank you.

Table of Contents

List of Tables

List of Figures

Abstract

Rotator cuff tears are a common cause of pain and disability due to injury and degradation of rotator cuff tendons. More than 250,000 patients require surgery each year, a majority of whom are over the age of 40. The current surgical treatments include tendon reattachment with surgical suture and graft transfer. It has been reported that the suture repair surgery has failure rates estimated between 20% and 70%, and the failure rate increased linearly with increased tear size. Thus, rotator cuff tendon repair remains a challenge in orthopedic surgery. Tissue engineered tendons, aiming at mimicking the intrinsic properties of natural tendons, have a great potential to replace the damaged human tendon. We propose a novel solution to engineer rotator cuff tendon by using the human amniotic membrane (hAM) as a scaffold with adipose-derived stem cells as a cell source. Cyclic mechanical stimulation is one of the key factors in tendon tissue engineering as it has been shown that it promotes tenocyte differentiation and mechanical properties of the tissue graft. The goal of this study is to develop a novel bioreactor that provides a tissue culture environment and controllable force and strain based mechanical stimulation.

Most of the current tendon tissue engineering bioreactors in use are custom made. Custom made bioreactors are less costly and more suitable for the tissue samples compared to the commercial bioreactors. Most of the custom made bioreactors provide strain based mechanical stimulation. One issue with strain based bioreactor is that some scaffold materials deform under certain mechanical stimulations. When deformation happens, the sample length changes, and the percent strain will not be precise anymore. Also, the initial position of the tissue sample in the bioreactor is not well calibrated. It is impossible to

adjust the tissue sample position precisely by human eyes. Since stretch displacement is often in millimeter range, the imprecise initial position will cause an inaccurate mechanical stimulation. Thus, a bioreactor system is designed with three programs to address these issues. A pre-stretch program is developed to adjust the tissue sample to any required position precisely. A strain based stretching program is used to provide cyclic mechanical stimulations with a constant strain and force monitoring. If the force decreases over time, it suggests that the tissue sample deformed and the strain is no longer accurate. In this case, a force based stretching program could to used instead to provide a constant force based mechanical stimulations to the tissue sample.

Furthermore, the variability of the mechanical properties of hAM was also studied with the use of a strain based program. The results show that hAM samples processed with the decellularization protocol have a consistent mechanical property at different positions. An extra 1.5% strain is suggested to added the tissue sample as the initial position before applying mechanical stimulation.

1. INTRODUCTION

1.1 Background and Significance

Rotator cuff tears, a common cause of shoulder pain and disability, are caused by injury and degradation of rotator cuff tendons. There are approximately 4.5 million doctor visits per year due to shoulder pain, and about 250,000 patients undergo surgery in the United States. A majority of the patients are over the age of 40[1]. Based on the size of rotator cuff tear, the surgical failure rates are estimated between 20% and 70%[2]. With the limitation of the current treatments, rotator cuff tendon repair remains a challenge in trauma and orthopedic surgery[3]. To improve the current treatment options, researchers have attempted to tissue engineer a tendon graft to replace the torn tendon. The tissue engineered tendon graft much be grown in a bioreactor and stimulated with mechanical stretching. While many designs for bioreactors and stretching protocols have been described in the literature, none have been developed that lead to grafts with mechanical properties similar to those of native tendon. The goal of this thesis is to propose and design a novel tendon bioreactor system that imposes a more uniform stretching protocol on the developing tendon.

1.1.1   Rotator Cuff and Rotator Cuff tendon

Rotator cuff is defined as a supporting and strengthening structure of the shoulder joint that is made up of the capsule of the shoulder joint blended with tendons and muscles as they pass to the capsule or across it to insert on the head of the humerus[4]. (Figure 1) In other words, the rotator cuff is a group of muscles and

tendons that act to stabilize the shoulder and allow the shoulder to move in different directions.
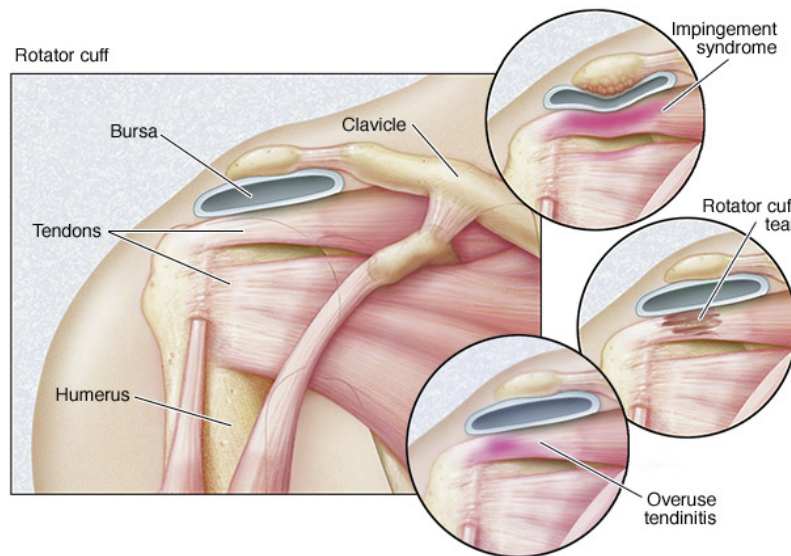
Figure 1. Rotator cuff and injuries[5].

Rotator cuff tendons are the soft connective tissues that connect and transmit forces from the muscle to the bone[6]. The main component of the tendon is water, which makes up 55-70% of the wet weight[7]. Tendons also consist of collagens, proteoglycans, glycoproteins, and cells. Among all these compounds, collagens are the major molecular components of the tendon extracellular matrix. Type I collagen is the most abundant tendon component, which constitutes about 60% of the dry mass of the tendon and about 95% of the total collagen[6, 8]. Tendons have a hierarchical organization (Shown in Figure 2), with the highly aligned collagen fibers arranged in a longitudinal manner, parallel to the mechanical axis, to develop a structure that has a high tensile strength[7] Each level of this collagen-rich hierarchy is interspersed with varying amounts of non-collagenous extracellular matrix[9]. Cells, present in low density, maintain and turn over the extracellular matrix of the tendon. Fibroblasts (tenoblasts and tenocytes) are the dominant cell types, although endothelial cells, synovial cells and chondrocytes are also

present in tendons[7]. However, compared to other cell types, the phenotype of the tendon

cells is still poorly understudied in general.
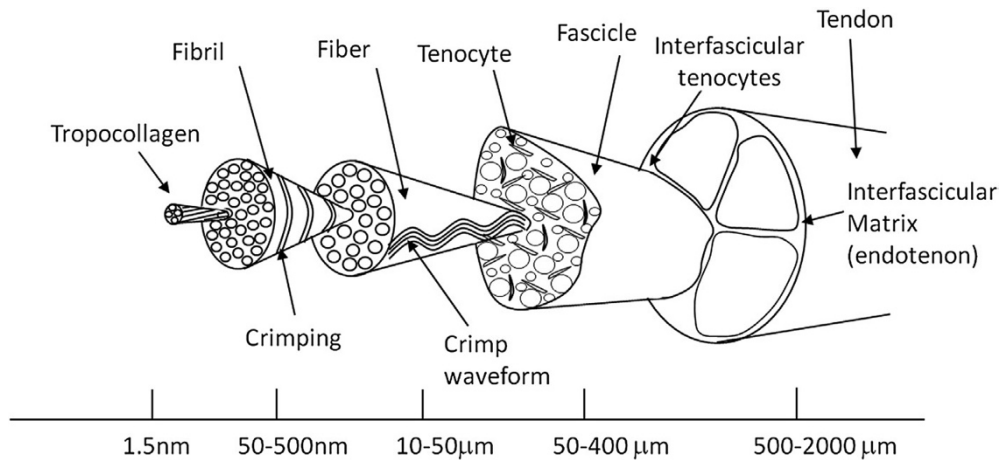
Figure 2. Schematic showing the hierarchical structure of tendon, in which collagen molecules assemble to form subunits of increasing diameter[10].

1.1.2 Rotator Cuff Injury

Rotator cuff tendon tears can be caused by many reasons: the natural degradation from

aging, overuse of shoulder from heavy lifting or sports, or an acute tear from an injury of

the shoulder.[5] Various types of people suffer from rotator cuff injury, especially

professional athletes, working age adults who might overuse shoulders, and elderly

people. Studies show that 30-50% of sports injury include an injury to a tendon, and more

than 67% of rotator cuff injuries occur in working age adults[3]. In addition to that,

approximately 21-27% of 60 year olds are affected by rotator cuff injury, and the

prevalence of rotator cuff injuries increases with age[11-13]. These numbers become

extremely significant with the increase of elderly participation in labor force and aging

of the U.S. population. The yearly rotator cuff injuries are only expected to increase in

the U.S. Thus it is important to have effective treatments for the patients.

1.1.3   Current solution

Injuries to the rotator cuff range from partial to full thickness tears with varying levels of functional limitations[14]. Two major treatments are available for patients currently: conservative treatments and surgical treatments. The selection of treatment depends on the tendon quality, tear size, tear location and so on. The conservative treatment includes rest, medication, and physical therapy. If the conservative treatment does not result in improvement of shoulder function, then surgical options are considered. There are three major surgical options for rotator cuff repair. One option is re-attaching the tendon to the head of humerus by surgical suture. Another option is tendon transfer with autograft. Although this involves sacrifice of some other healthy tendon of the patient, the autograft remains the gold standard for surgical procedure[15]. The last option is allograft transfer, which is graft transplantation to replace the injured tendon with a patch (shown as Figure 3). The most commonly used commercial available tendon patches are the Zimmer Collagen Repair Patch (Tissue Science Laboratories, Covington, GA), GraftJacket (Wright Medical Technology, Inc.), and they are obtained from porcine skin and human skin[16].
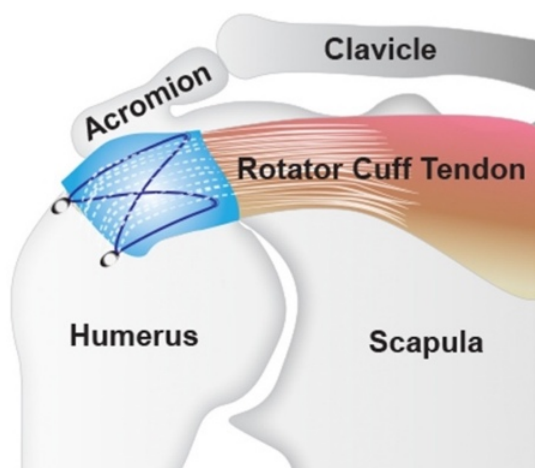
Figure 3. Rotator Cuff Repair with a tissue Patch[17]

However, the treatment outcome of rotator cuff injury is still limited. The graft transfer surgeries usually result in fibrotic tissue with low mechanical properties compare to native tendon, the commercial tendon patches serve limited mechanical role in rotator cuff repair[18, 19]. The young's modulus of GraftJacket and Zimmer Collagen Repair Patch, tested in vitro, are 48.09±49.56 and 68.85±7.99 MPa [20], comparing to the young's modulus of human rotator cuff to be 165 ±20 MPa[21]. The suture repair surgery failure rate is estimated between 20% to 70%, depending on the tear size and site[22]. The repaired tendon still has inferior biomechanical properties compared to the original tendon tissue. Researchers from the Orthopedic Research Institute in Kogarah, Australia studied the relation between tear size and re-tear over 500 patients [23]. The surgical failure rate increased linearly with increased tear size: ≤2 cm (10%), 2 to 4 cm (16%), 4 to 6 cm (31%), 6 to 8 cm (50%), and >8 cm (57%). Another research group did the same study over literature review and conclude that the small to medium rotator cuff tear (1-3cm) has a re-tear rate of 22±7%; large tear (3-5cm) has a re-tear rate of 46±21%; Massive tear (2 or more tendons) has a re-tear rate of 58±12%[24]. Other studies found that patients with an intact rotator cuff 6 months after the surgery were much less likely to experience a re-tear than those whose rotator cuff was not completely intact. Some factors that can decrease the likelihood of a satisfactory result are: poor tendon/tissue quality, large or massive tears, poor patient compliance with rehabilitation, and patient age (older than 65 years).

1.2 Tissue Engineering Approach

With the often unsatisfying surgical outcome, investigators have turned to tissue engineering to bring hope of revolutionizing treatments and therapies for many patients

who suffer from failing tendons. Tissue engineering, also called bioengineered tissues, is the replacement, repair, and regeneration of tissue. The goal of tendon tissue engineering is to develop a functional tendon replacement in vitro, and then implant it in vivo in place of other graft materials. The tissue engineered graft is expected to have a better mechanical property compare to the current commercial available graft materials. There are three key components in tissue engineering. The first one is the selection of the appropriate cell type. The second key component is the development of a suitable scaffold or matrix to support cell attachment. The last one is the provision of a controlled environment, along with suitable biochemical and physicochemical factors, to allow the cells to proliferate and differentiate to appropriate tissue structures[25].

The general tissue engineering procedure outline is shown in Figure 4; the first step is cell sourcing, which is the isolation of some appropriate type of cell from the patient. The second is step is cell cultivation and proliferation, which is preparing cells so that they are ready for the seeding procedure. The third step is tissue development, which involves cell seeding, cell attachment, and cell differentiation. Mechanical stimulation and molecular signaling are the two common environmental factors that promote cell differentiation. The last step is construct implantation, which is implanting the engineered tissue back to the patient.
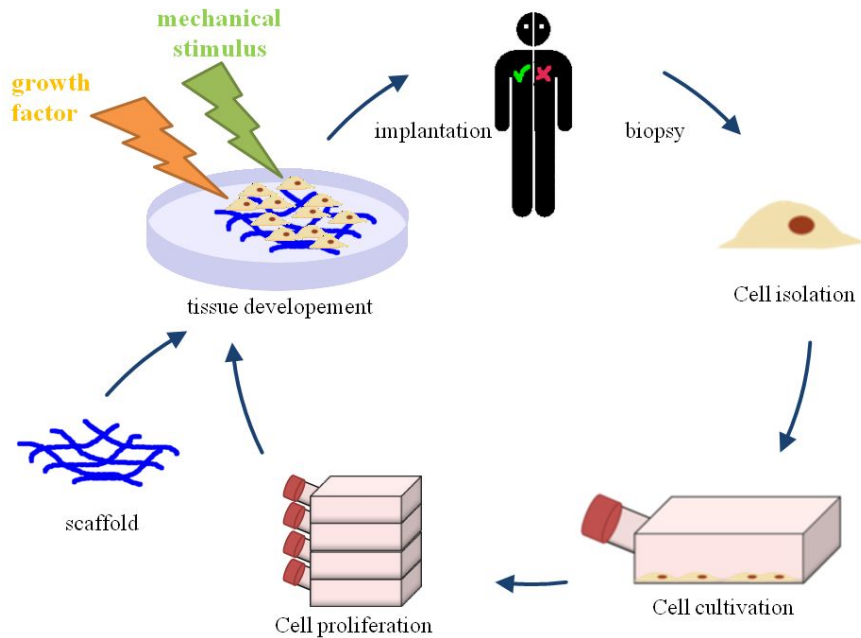
Figure 4. Principle of Tissue Engineering

1.2.1 Cell Source: ADSCs, BMSCs, and TSPCS

Even though tissue engineering has so much potential in the treatment of failing tissues
and organs, it is still facing some critical issues. One is the cell source selection between
autologous cells and allogeneic cells. Allogeneic can provide for an off-the-shelf product
or strategy, but in many cases will need to employ a strategy for engineering immune
acceptance[3]. On the other hand, autologous cells have no issue with immunogenicity,
but it is a less reliable tissue engineering product. There are different types of autologous
cells that have differentiation potential. Adipose derived stem cells (ADSCs), bone
marrow-derived stem cells (BMSCs), and tendon stem/progenitor cells (TSPCs). Each
cell type has its biological advantages and limitations; ADSCs are present in great quality
in adipose and are easy to isolate; BMSCs are the best characterized and most widely
used stem cells in tissue engineering[3], but it is a highly invasive procedure to get them
compared to the adipose cells; and TSPCs, a reported and characterized cell type in

7

2007[26], have been shown to have great self-renewal ability, cell proliferation, and tenogenic differentiation potential [27]. The TSPCs have disadvantages as well, such as their scarcity in tendon tissue and a risk of morbidity at the tissue extraction site[15]. Thus the cell source should be carefully picked for different tendon tissue engineering studies.

1.2.2 Scaffold Materials: biological and synthetic

The other critical issue of tendon tissue engineering is the selection of the scaffold. The cell phenotype varies depending on the microenvironment around the cell, and the microenvironment includes both biomechanical and biochemical components, as well as the cell's extracellular matrix[28]. Therefore, it is important to choose the right type of scaffold, either a biological material or a synthetic material, as well as the size and shape of the scaffold, in order to provide an appropriate cell seeding environment. Natural tendon mostly consists of collagen; therefore, a collagen-based tissue construct has been most studied for tendon tissue engineering.

Biological scaffolds are often obtained from mammals, such as human, pig or cow. Most of the commercially available extracellular matrix scaffolds for rotator cuff tendon repair are decellurized mammalian tissue such as human epidermis, porcine dermis and porcine small intestinal submucosa (SIS) [29]. They are often chosen because these tissues are collagen rich, and the natural collagen fibers are beneficial for cell attachment[30]. However, the biocompatibility of non-human derived biological material have been called into questions. For example, Negative clinical results of porcine SIS product have been reported saying 60% patients in one study showing inflammation after implantation [31]. Biocompatibility of non- human derivative tissue is not well understood, and need

8

further studies. Polylactic acid (PLA), poly-L-lactid acid (PLLA), polyglycolic acid (PGA), poly-D, L-lactic-co-glycolic acid (PLGA) are the commonly used polymers for synthetic scaffolds. Synthetic scaffolds are more homogeneous compared to biological scaffold. However, they have lower biocompatibility because of frustrated phagocytosis and inflammation[17]. Synthetic scaffolds also have a rapid degradation rate and potential risk of acidic byproducts including toxic polyester[32].

Hydrogels are also a popular option as tendon tissue engineering scaffolds. Hydrogels are a network of natural or synthetic polymer chains with significant water content, and it can have similar structure to the extra cellular matrix of natural tendon. Hydrogels can be formed from both synthetic and biological material. However, naturally derived polymers, such as collagen, fibrin, gelatin, agarose, alginate, chitosan, and hyaluronic acid (HA) are most commonly used[33]. Hydrogels have good biocompatibility and mass transport properties but limited mechanical properties. Thus hydrogels are often combined with other biological and synthetic scaffold to develop a tissue patch.

1.2.3   Human amniotic membrane

The biomaterial of choice selected for this study is decellularized human amniotic membrane (hAM). Human amniotic membrane is the most inner layer of human amniotic sac. It has several layers: epithelium, basement membrane and an avascular stroma which includes a compact layer, a fibroblast layer and a spongy layer.[34] The decellularized hAM used in this study is the basement membrane obtained with a decellularization protocol (described in detail in section 4.1.1). hAM is a commonly used biomaterial in the medical field. The extracellular matrix components of the basement membrane of the hAM create an almost native scaffold for cell seeding in tissue engineering.[34]

hAM has limitations as well. Both intradonor and interdonor variation have been reported[35]. Interdonor variations in the membrane biochemical (protein amount and grow factors) composition and structure have been reported in relation to age, race, maternal health and diet of the donor, as well as fetal sex, health and gestational age[35, 36]. Connon et al. reported that the variations in thickness, transparency and refractive index of hAM depended on processing methods used and the site of the sample, whether close to the placenta or close to the umbilical cord[35, 37]. It was suggested that standardization of the processing protocol helped reduce the variance in chemical composition and mechanical properties[38-40].The variability of the mechanical properties of hAM were performed in this study with experiments to make sure all the cells are experiencing the same mechanical properties.

1.2.4   Mechanical Stimulation

Mechanical stimulation is another key factor in tendon tissue engineering. When a collagen based construct is mechanically constrained, the collagen fibrils align in the direction of constraint, and a highly aligned, compacted collagenous construct can thus be fabricated[2]. The collagen fibers can therefore be manipulated into desired structures using appropriate mechanical stimulations. Furthermore, fibroblasts can generate contractile forces in the culture regulated by external mechanical forces[8]. The contractile forces generated by fibroblasts in collagen constructs have been studied for years, and it has been shown that the external mechanical forces can regulate both fibroblast contractile forces and matrix production. This means that mechanical stimulation of tendon constructs, when done in a way that mimics the in vivo tendon

activity, could improve the construct microstructure and mechanical properties. The cell growth, extracellular matrix (ECM) production, and the mechanical properties of collagen constructs, indeed appear to be related directly to the application of the cyclic strain. Therefore, one of the major goals of the bioreactor for tendon tissue engineering is to provide cyclic mechanical stimulation.

Two types of mechanical stimulation, static tensile load and dynamic stimulation have been studied so far, and it has been shown that dynamic strain is more beneficial than static tensile load[3]. A study with an MSC-seeded PLGA construct shows that there is no significant difference in collagen synthesis or cellular proliferation when comparing static load to the unloaded control group. It is known that dynamic stimulation benefits more collagen synthesis and cell differentiation. However, the stretching parameters, such as the amount applied strain, duration, and frequency, still need to be optimized.

In terms of strain, between 1% and 5% have been shown to increase cell proliferation, gene expression of tendon related genes, tissue formation, and mechanical properties, such as tensile strength, stiffness, and elastic modulus[32]. The physiological range of human tendon is under 4% strain, and microscopic failure occurs when the tendon is stretched out of the physiological range[41, 42]. Thus, as we want to closely mimic nature tendon activity, the mechanical stretching strain should be under 4% strain. In terms of frequency, a frequency of 0.1 Hz and 0.25 Hz were most beneficial depending on the pattern of stimulation, which was concluded by Joshi and Webb research group[43]. Thus an ideal bioreactor system should be tunable for studying the appropriate stretching strain, frequency and duration.

1.3 Bioreactor System Review

Bioreactors are used to provide a tissue culture environment and mechanical stimulations in tendon tissue engineering. Both commercial bioreactors and custom-made bioreactors have been used by different research groups. A bioreactor could be incubator based or independent. The independent bioreactors do not need to be placed in the incubator to obtain proper culture conditions such as temperature and CO_2 concentration.

So far, all the bioreactors that have been used for studying tendon engineering include one or more culture chambers and a mechanical stimulation system. The culture chamber is essential because it provides a sterile environment for tissue culture. A mechanical stimulation system is beneficial for fiber aliment and cell differentiation. A strain based stimulation system provides stretching to a certain displacement, and a force based stimulation system provides stretching to a certain force. Sub-systems, such as medium circulation system, medium monitoring system, mechanical stimulation system, sample monitoring system, and feedback system, were selectively added to the bioreactor system by different research groups. The medium circulation system is used to circulate, mix, and change medium. A medium monitoring system is often included with an independent bioreactor since they are not placed in an incubator. Sample monitoring systems, either monitoring force or displacement, are used to observe the tissue sample condition. Feedback systems, which are the least commonly used, provide force or strain feedback to the bioreactor system. The feedback is then used to adjust the mechanical stimulation. Wang et al. reviewed bioreactors used by twelve different tendon tissue engineering research groups in 2012[32]. Eight other tendon bioreactors systems published from 2012 to 2018 are combined with Wang et al.'s study and listed in Table 1. From total of 20

research teams, only two teams used constant force bioreactors [44, 45], the rest were all custom made bioreactors with or without a monitoring system. Strain based bioreactors are relatively easy to make. One issue with the strain based bioreactor is that, if permanent deformation of the tissue samples occurs after applying mechanical stimulation, the percent strain will not be accurate anymore since the tissue length has changed. The force based bioreactor used by the two research groups was a commercial bioreactor called LigaGen, which is discussed in section 1.3.2. Three other representative custom-made bioreactors will also be discussed in the following sections to compare the pros and cons for each type of bioreactor.

Table 1. Bioreactor review

First Author	Bioreactor Type	Mechanical Stimulation Type	Effect	Reference
Altman (2002)	Custom-made step motor bioreactor with environmental chamber	Strain based	Cell density increase	[46]
Juncosa-Melvin (2006)	Custom-made pneumatic cylinder bioreactor with LVDT for displacement monitoring	Strain based	Stiffness increase	[47]
Webb (2006)	Custom-made step motor bioreactor	Strain based	Stiffness increase	[48]
Androjna (2007)	Custom-made bioreactor with load-displacement measure system	Strain based	Cell density increase Stiffness increase	[49]
Nirmalanandhan (2008)	Custom-made pneumatic cylinder bioreactor	Strain based	Stiffness increase	[50]
Nguyen (2009)	Custom-made linear actuator bioreactor with load cell for force measurement	Strain based	Improved fiber orientation	[51]
Abousleiman (2009)	Custom-made linear actuator bioreactor with medium circulation system	Strain based	Elastic modulus increase Cell proliferation	[52]
Butler (2009)	Custom-made pneumatic cylinder bioreactor with LVDT for displacement monitoring	Strain based	Stiffness increase	[53]
Chen (2010)	Custom-made step motor bioreactor	Strain based	Collagen increase Better cell alignment	[54]
Doroski (2010)	Custom-made linear motor bioreactor	Strain based	Collagen increase	[27]
Saber (2010)	Ligagen L30-4C (Tissue Growth Technologies)	Force based	Stiffness increase	[44]

Woon (2011)	Ligagen L30-1C & Ligagen L30-4C (Tissue Growth Technologies)	Force based	Elastic modulus increase	[45]
Bilgen (2013)	Custom-made step motor bioreactor with load cell (force feedback) and linear optical encoders (position feedback)	Strain based	Elastic modulus increase Proteoglycan deposition	[55]
Wang (2013)	Custom-made step motor bioreactor	Strain based	Cell proliferation	[56]
Laurent (2014)	Custom-made motor bioreactor with strain gauge record the sample deformation	Strain based	Cell proliferation	[57]
Goodhart (2014)	Modified BOSE Electro force 3200	Strain based	Cell proliferation ECM production increase	[58]
Youngstorm (2015)	Custom-made step motor bioreactor	Strain based	Elastic modulus increase	[59]
Qin (2015)	Custom-made step motor bioreactor	Strain based	Tenogenic differentiation Cell infiltration	[60]
Cook (2016)	Custom-made linear step motor bioreactor with load cell for force monitoring	Strain based	Cell proliferation	[61]
Wu (2017)	Mechano Culture T6 Mechanical Stimulation System	Strain based	Cell proliferation and infiltration Tendon-specific genes expression Fiber alignment	[62]

1.3.1 Initial position issue

In the process of reviewing different bioreactor systems, it became clear that most research groups did not address how they adjust the tissue samples to the initial position. The initial position is the degree of tension in the sample before performing mechanical stimulation, and it is often adjusted by human eyes or feeling from hands. Sample initial position adjustment is a critical issue to strain based mechanical stimulation because an inaccurate initial position can cause the stretching strain to be inaccurate. As an example, Figure 5 shows a hAM sample (Length=75mm) at different positions. The hAM sample in Figure 5A was at its original length, 0% strain is added. Figure 5B shows the sample being stretched by 1.5mm (2% extra strain). As we can see from the two figures, it was

very hard to notice the 1.5mm difference with human eyes. If the researcher wants to perform mechanical stimulation on this sample from its original length, and adjust the sample position only by observation, there is a large chance that the initial position will be off. A 1.5mm displacement off will cause the strain to be off by 2%. Since the mechanical stimulation for tendon tissue engineering is in small strain range, even 1% off is non-negligible.

A.   **B.**
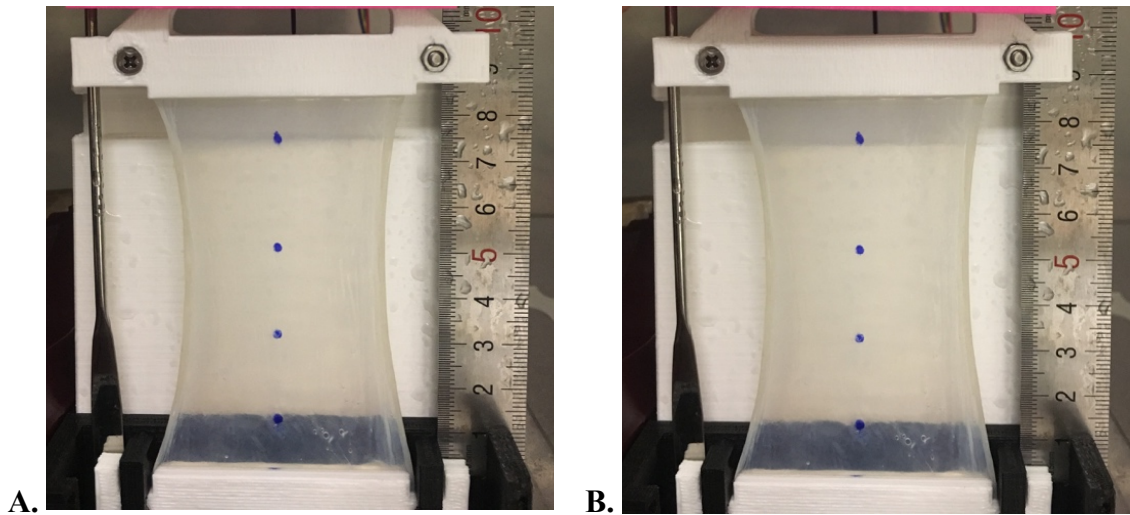
Figure 5. hAM sample at different positions.
A. Orgianl length (L=75mm, 0% extra strain) B. Stretched by 1.5mm (L=76.5mm, 2% extra strain)

1.3.2   *Force Based Commercial Bioreactor*

Shown in Figure 6 is the most common commercially available bioreactor, the LigaGen Tension Bioreactor System (Bangalore Integrated System Solutions (P) ltd. Karnataka, India). LigaGen uses a tension/compression mechanical stimulator, which controls both load and displacement[63]. Two research groups, Saber[44] and Woon[45], have used LigaGen to provide force based loading to the tissue sample. A software and control platform GrowthWorks is provided to create the stimulation profile and monitor graphical

displays and sample stiffness. Two different chambers can be chosen to fit either a single sample or multiple samples (two or four).
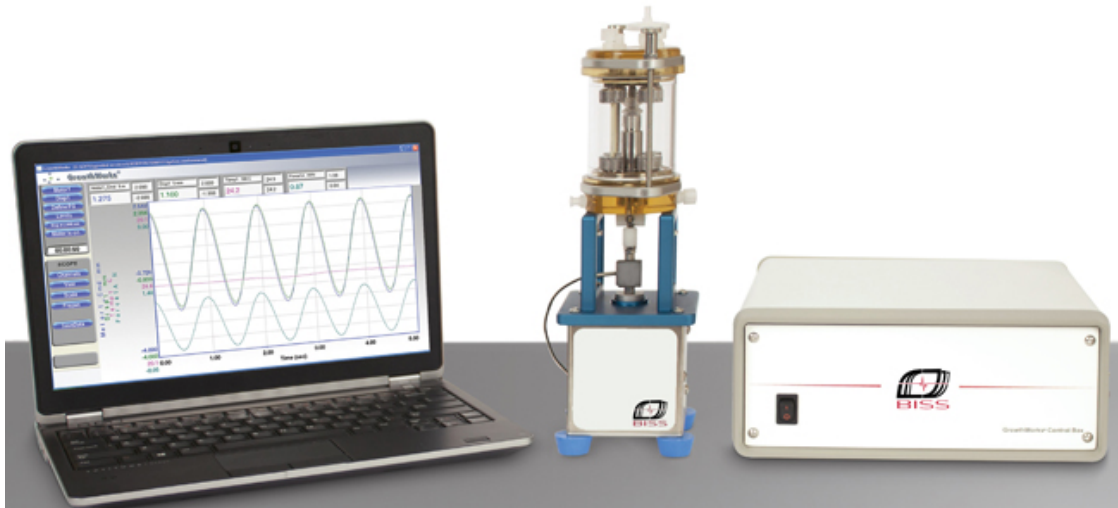
Figure 6 Overview of LigaGan: Tension Bioreactor System[63].

There are still some limitations to this bioreactor system. The size of sample placed in this chamber is limited to 30mm in length, and 3mm in width. Also, it is very costly. The L30-1C costs 50,000 US dollars, and the L30-4C costs 60,000 US dollars. Thus, compared to the commercially available bioreactors, custom-made bioreactors are more popular in the tendon tissue engineering field. Custom-made bioreactors are less costly and more flexible towards the tissue sample size and quantity.

1.3.3 Strain-based Bioreactor with Stepper Motor

A research group from Mayo Clinic studied the effect of mechanical stimulation on bone marrow stromal cell-seeded tendon slice constructs, in order to develop engineered tendon patches for rotator cuff repair[60]. The constructs were prepared with 40 mm decellularized dog Achilles tendon slices and dog bone marrow stromal cells, and subject to cyclic stretching (3% strain at 0.2Hz, 20 minutes/hour) for 1, 3, or 7 days. The

16

mechanical properties, morphologic characteristics and tendon-related gene expression of the constructs were investigated. The results show that the gene expression of type 1 collagen significantly increased in the stretching group compare to the unstrained control group.

The bioreactor, shown in Figure 7, is a strain based mechanical stimulation system, and the stretching is provided by one stepper motor. This bioreactor included three culture chambers with four samples in each. All 12 tissue samples were stretched with a displacement of 1.2mm (40mm× 3%) at the same time. The tendon tissue constructs are soft and flexible. For small displacements, when the construct is placed into the culture chamber, it is very difficult to determine if the sample is initially at the zero strain position. If the sample is being stretched for only 1mm before adding mechanical stimulation, the actual percent strain then becomes 5.5% instead of 3%. This system also lacks a monitoring system to check the tissue sample condition.
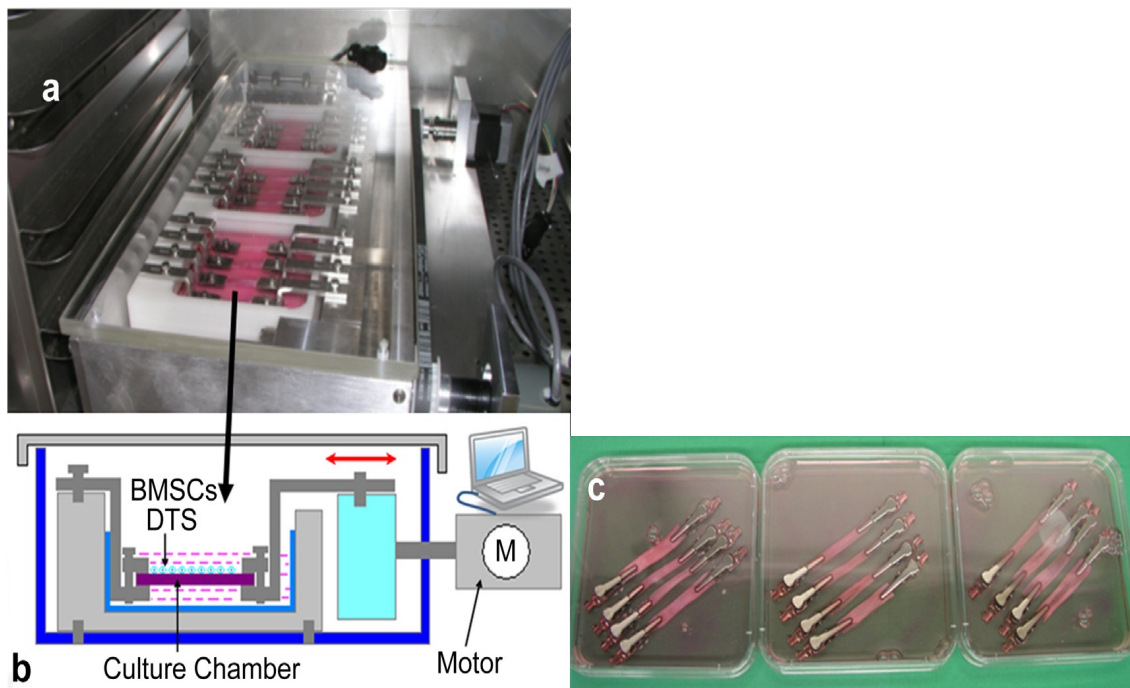
Figure 7 Overview of bioreactor design by Mayo Clinic research group.[52]

The third bioreactor system is designed by a research group from the University of Oklahoma. The tendon tissue constructs were prepared with decellularized human umbilical veins, type I collagen, and bone marrow MSCs from male Wistar rats. Over the years, this group investigated the effect of stretching parameters, initial cell density, and tenocytic extract on tissue sample mechanical and biological properties. The set up of the bioreactor they were using is shown in Figure 8a.

Figure 8. Bioreactor setup for tendon tissue engineering from OU research group[52].

This bioreactor system consists of a dual linear voice coil motor (Figure 8b), which can exert displacement for extended time periods in either direction along the vertical axis,

providing cyclic mechanical stimulation[51]. A signal converter and an amplifier (Figure

8c) were used to control the motor movement. The direct inputs to this motor are voltage

and frequency. Voltage input corresponds to displacement and frequency corresponds to

stretching time and speed. Three culture chambers house individual tissue constructs

(Figure 8d), and the constructs were connected to the actuator through a triangular plate.

With this plate on top, each tissue construct is guaranteed to be stretched at the same force.

The advantage of this bioreactor is that it includes a medium circulation system. It not

only circulates the culture medium, but also changes medium without moving the

bioreactor out of the incubator. This avoids potential contamination and damaging of the

tissue construct that might occur while moving the constructs. However, the three

individual culture chambers are connected together through the media reservoirs, which

will increase the chance of tissue cross contamination. Also, the initial position of the

tissue samples was adjusted by human eyes observation, which will not be accurate and

would affect the accuracy of the mechanical stimulation.

1.3.5   *Force based bioreactor with feedback system*

A custom made incubator-based bioreactor was developed by a research group studying

the tendon response to mechanical loading[64]. This bioreactor is able to provide force

based load to the tissue sample. Shown in Figure 9, an electromagnetic linear actuator

and its controller provides mechanical stimulation, a load cell measures the force added

to the tissue samples, and an optical encoder is used to detect the linear position. In

addition to that, Field-programmable gate array (FPGA), a reprogrammable silicon chip,

is used to acquire force feedback from the load cell, and govern the motor controller with

the feedback data. Samples were divided into four groups. Except for the control group of no load, the samples from the other three groups were stretched cyclically with a stress of 1.5Mpa. The second group stopped the stretching when they reached 4% strain, the third group stopped at 8%, and the last group stopped when the tissue sample was ruptured. Even though this bioreactor is not being used specifically for tissue engineering in this study, it has potential to provide cyclic mechanical stimulation. This bioreactor provides mechanical stretching based on force or stress, which is not common since most of the custom designed bioreactors provide stretching based on strain. The force based bioreactor must include a feedback system, either within the motor itself, or in cooperation with a load cell. In this case, the load cell is included in the feedback system. In addition, an optical encoder is also included to detect the position, which helps to determine the percent strain to which the samples were being stretched. One advantage of the FPGA chip is that it can interface with LabVIEW software. With a custom written program, it is possible to turn this bioreactor to a force based stimulation system that provides tunable cyclic stretching to the tissue sample.
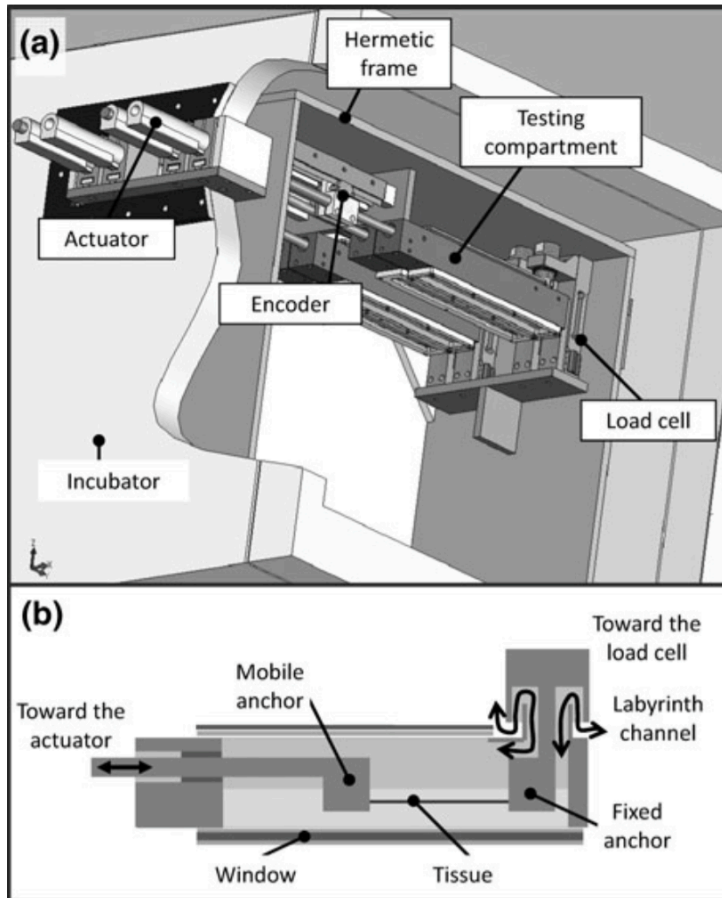
Figure 9. overview of bioreactor from Mayo Clinic research group[64]

To our knowledge, there is no custom made bioreactor that is able to provide cyclic force based mechanical stimulation along with a monitoring system. Most of the bioreactors that have been described in the literature are strain based, with or without a force and displacement monitoring system.

1.4 Thesis objectives

1.4.1 Hypothesis

Based on the poor outcomes of current best available treatment options for severe rotator cuff tears and the preceding literature review, we propose a novel solution to engineering rotator cuff tendons by using the human amniotic membrane (hAM) as scaffolds, and a bioreactor to help with tendon tissue development.

1.4.2 Objective 1: Design a bioreactor with force and strain based stretching programs

The first objective sought by this project is to develop a bioreactor system for tendon tissue engineering that can provide tissue culture environment, and a tunable constant force or strain based cyclic mechanical stimulation. The current available bioreactors are either strain based or force based. Thus, we want to develop a bioreactor that can measure the force corresponding to the percent strain, and stretch the sample to that force.

1.4.3 Objective 2: Study the degree of variability of the mechanical properties of hAMs

The second objective is to study the variability of the mechanical properties of hAMs. The ideal condition is that all the tissue samples have the same properties and can be stretched to the same degree at all positions, so that cells are experiencing the same mechanical properties. However, intra-donor and inter-donor variance of hAM have been reported. Thus, it is necessary to quantify the variability of the mechanical properties of the hAMs processed with our protocol.

1.4.4 Objective 3: Adjust the initial position of tissue sample consistently

The third objective was to design a pre-stretch program that can make sure the samples have a consistent initial position. Thus, instead of having the initial position inaccurately determined by human eyes or feeling from hands, a pre-stretch program is needed to help adjust the tissue sample to an accurate initial position.

2. BIOREACTOR PARTS AND DESIGN

2.1 Material and Method

2.1.1   Design Criteria

In order to design a tendon tissue engineering bioreactor that provides both strain based

and force based mechanical stimulation, several design criteria were followed. First of all,

the bioreactor system must provide a clean and stable environment for tissue culture, and

this can be accomplished by having a culture chamber and media circulation system.

Second, this bioreactor system must provide mechanical stimulation in order to promote

cell differentiation. Third, the mechanical stimulation parameters (a partial list includes

stretch time, frequency, and amplitude) must be tunable for tendon tissue engineering

study. Fourth, a monitoring and feedback system must be included in order to provide

force based mechanical stimulation. Finally, the whole bioreactor must be able to fit in

the incubator, and all electrical and mechanical components must be functional in the

incubator (37°C, 5% CO_2).

The bioreactor design is shown in Figure 10. In order to achieve the criteria, stepper

motors (SM-42BYG011-25, SparkFun® Electronics, Colorado, USA) were used to

provide mechanical stretching, and 5 kg micro load cells (CZL635, Phidgets, Calgary,

Canada) were used to continuously measure the force applied to the tissue samples. The

tissue sample was held by two clamps at the top and bottom, and placed into the tissue

culture chamber. The size and shape of the chambers were designed based on the sample

size and other requirements, such as minimizing the medium usage, and then 3D printed.

The top clamp was linked to the stepper motor through a pulley with stainless steel wire

(diameter=0.23mm) The pulley was connected to the load cell with a screw. A media

circulation system was developed for circulating and changing media. An Arduino control board (A000066, Arduino ™, UNO, Torino, Italy) and the software LabVIEW (National Instruments ™, Texas, USA) were used to run custom written programs that offered adjustable cyclic mechanical stimulations to the tissue sample based on strain and force. The programs designed for running this bioreactor will be discussed in the next chapter.
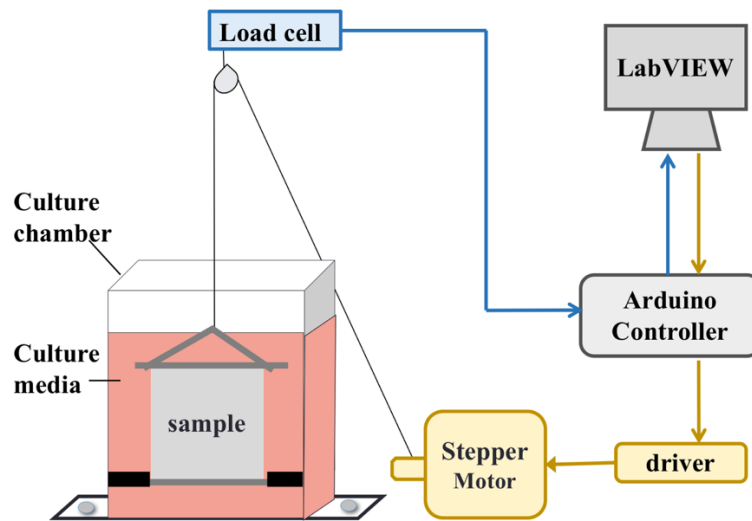
Figure 10. Sketch of the one channel bioreactor system.
Load cell related parts are colored blue, and stepper motor related parts are colored yellow.

2.1.2 Bioreactor body frame design

The bioreactor consisted of a body frame, four culture chambers, four media reservoirs, and two peristaltic pumps (one for medium circulation and one for medium change). The body frame of the bioreactor was responsible for stabilizing the operation of the system. Two acrylic boards (60cm×30cm) and four stainless steel rods (40cm) were used to construct the body frame. The bioreactor layout is shown in Figure 11A. Four stepper motors were fixed onto the bottom frame through brackets. The culture chambers were removable, and were secured to the bottom frame with screws. Each tissue culture

chamber was connected to a medium reservoir individually with 3 types of tubing (details about the tubing will be discussed in section 2.1.1.1). A peristaltic pump was placed next to the body frame to circulate the culture media. Load cells were fixed onto the top frame with brackets, as shown in Figure 10B. Each pulley was connected to its load cell with screws. As the shaft of the stepper motor rotates, the steel wire wraps around the shaft stretching the tissue sample through the pulley. Since the pulley is connected to the load cell, the force can then be measured.
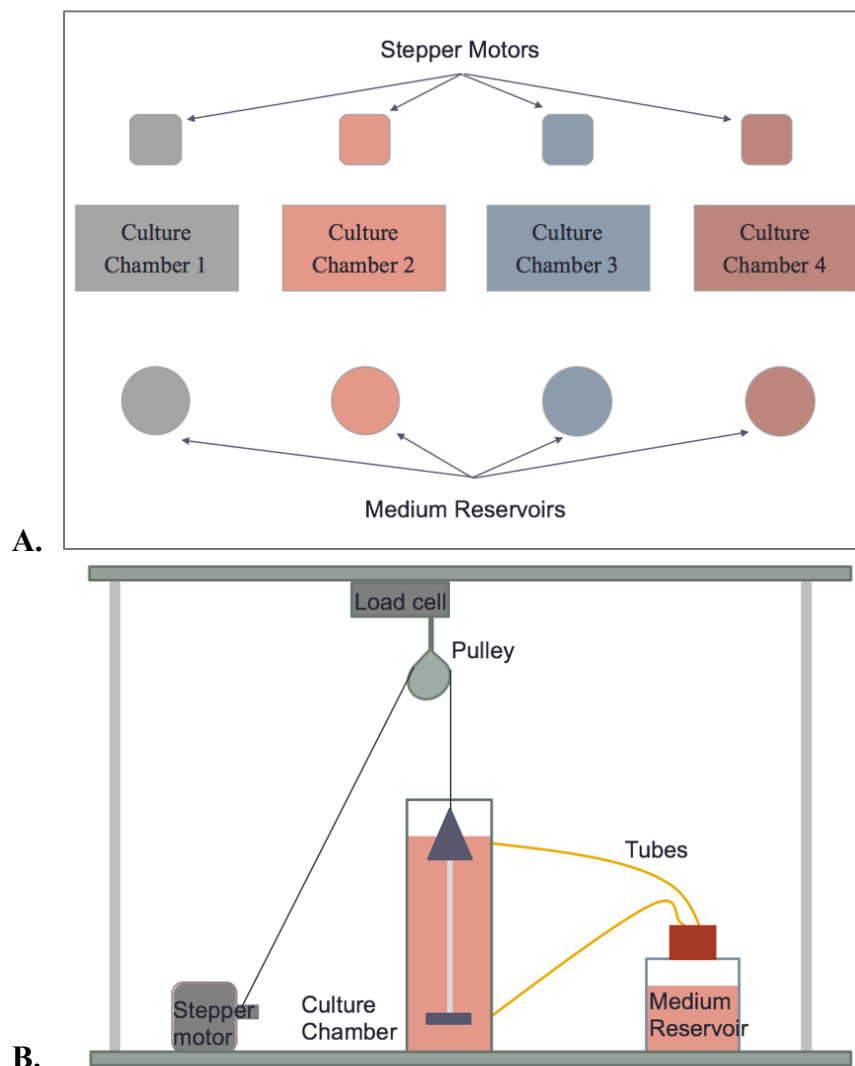
Figure 11. Overview of bioreactor body frame setup.
A: Top view of four channel bioreactor setup. B: Side view of the setup. (The peristaltic pump is not shown in this view for clarity)

25

2.1.3   Culture Chamber and Clamps Design

2.1.3.1 Chamber

The tissue culture chamber was designed as two separate pieces for the convenience of printing using the 3D computer-aided design (CAD) software named SoildWorks (Dassault Systems, Massachusetts, USA). The SolidWorks design file was then uploaded to the 3D printing software Ultimaker Cura (Ultimaker B.V., Amsterdam, Netherlands), which controlled the location and position within the 3D printer where the culture chamber would be printed. Figure 12 shows the view of the chambers within Ultimaker Cura. Figure 12A shows the two parts of the bioreactor chamber with the bottom part in front and the top part in back. Figure 12B shows the top view of the two chambers. The clamp that holds the tissue sample in the chamber was attached to the chamber using a hook shaped design that is visible in the bottom part of the chamber. The dimensions of the top chamber are 100×30×109.5 mm. The dimensions of the bottom chamber are 100×30×44 mm with the base length of 145mm. The thickness of the chamber is 5mm, and the inside volume of a fully assembled culture chamber is 180ml.
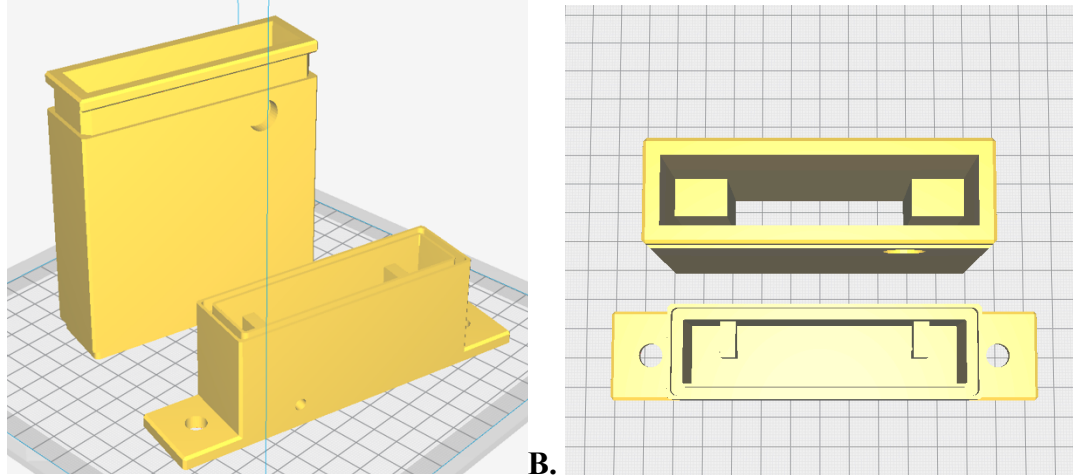
Figure 12. View of the bottom and top chambers within Ultimaker Cura.
A. Front view. B. Top view. The size of the grid is 10×**10**mm. The dimension of the top chamber is 100×30×109.5 mm. The dimension of the bottom chamber is 100×30×44 mm with the base length of 145mm.

Two holes, one at the bottom (diameter=4.5mm) and one at the top (diameter=12.5mm), were designed to connect with tubes for tissue culture medium circulation. Fresh medium from the reservoir was pushed to the culture chamber through the bottom hole by a peristaltic pump (Masterflex L/S®, Cole-Parmer, Illinois, USA), with a flow rate of 15ml/ minute. Extra medium in the culture chamber would flow out through the top hole and return to the culture media reservoir by gravity. The top hole was designed to have a larger diameter to help the extra medium flow out without additional applied pressure. The tubing size and other pump related parts information are listed in Table 2. The tubing used under the pump was a different material, for it can last longer under the pump head squeezing pressure.

Table 2. Description of Pump related parts.

All of these products are from Masterflex L/S®, Illinois, USA

	Model No.	Description
Pump Drive	ZM-7523-70	Brushless variable-speed digital drive; drive and control pump status
Pump Head	ZM-7519-06	8-channel, 4-roller cartridge pump head
Bottom Tubing 1	ZM-96410-16	Platinum-cured silicone tubing; connecting the bottom hole to reservoir
Tubing under pump head	ZM-06508-16	PharMed® BPT Tubing; use as the tubing under cartridge
Top Tubing	ZM-96410-17	Platinum-cured silicone tubing; connecting the top hole to reservoir
Cartridge	ZM-07519-70	large cartridges for 07519-06 pump heads; hold tubing onto the pump head in place

The culture chambers, both bottom and top, were printed with a desktop 3D printer (MP07325, MakerBot Replicator®, NY, USA) from OU library with white polylactic acid (PLA) (MP05612, MakerBot Replicator®, NY, US). XTC-3D® (B01BKSLI9M, Smooth-On Macungie, PA, USA), a formulated epoxy resin was used for coating both inside and outside of the culture chamber to smooth the surface and prevent leaking. Epoxy gel (B000DZD0HC, Loctite®, Düsseldorf, Germany) was used to glue the bottom and top part of the chamber together. Epoxy gel has been used by Mussett et.al., and there was no evidence showing biocompatibility issues.[65] Figure 13 shows a fully assembled tissue culture chamber, the top chamber part was printed with white PLA, and the bottom chamber was printed with black PLA. A glove and a zip tie were used to seal the top of the culture chamber after placing the construct.

Figure 13. Printed bioreactor chamber. The top part of the chamber was printed with while PLA and the bottom was printed with black PLA.

2.1.3.2 Clamps

The clamps that were used to hold the tissue samples were also custom designed and 3D printed with PLA. Two sets of clamps were used to hold one tissue sample, the top clamp set (85×62.5×4.4 mm) and the bottom clamp set (80×14×4.4mm). Each set of clamps consisted of two identical clamp pieces. Shown in Figure 14 are the front and back design of the top and bottom clamp pieces. After the clamps were printed, one M3 Hex nut was glued into each clamp piece.

Figure 15 shows how the tissue sample was placed between the two clamp pieces, and screws and nuts were used at the edge to hold the two clamp pieces together. The clamps were able to immobilize the tissue samples and prevent slipping. A hook, as shown in figure 15A, was connected to the small hole on the top of the clamp with steel wire. This hook was then used to attach the clamp to the wire, which in turn connects to the stepper motor.
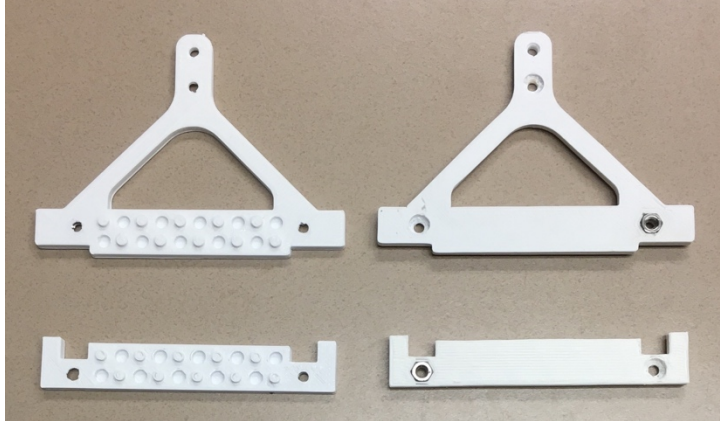
Figure 14. 3D Printed Clamps.
Top left: the front of top clamp. Top right: the back of the top clamp. Bottom left: the front of bottom clamp. Bottom right: the back of bottom clamp. The dimensions of the top clamp are $85 \times 62.5 \times 4.4$ mm, and the dimensions of the bottom clamp are $80 \times 14 \times 4.4$ mm. Each part of each clamp has a stainless steel M3 Hex nut glued in to it as shown.
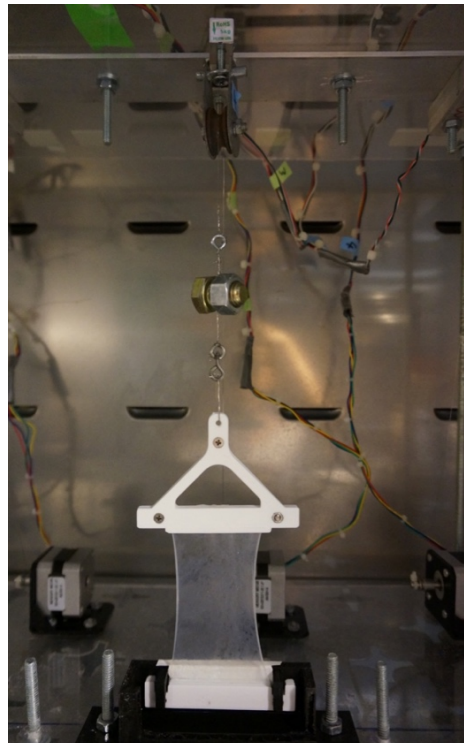
A.   **B.**

Figure 15. Clamps holding a tussue sample.
A: on table. B: in a bioreactor setup.

2.1.4 Correlation between applied displacement and actual displacement

Tissue samples were stretched by the rotation of the stepper motor drive shaft through a set of connections including steel wire, clamps and a hook. A stainless steel wire is elastic and will stretch when force is applied, and the elastic character of clamps and hooks are unknown. The wire stretching might not be negligible since the displacement of the tissue sample is in millimeter range. Thus, it is necessary to determine the amount of applied displacement that goes to the sample and amount of applied displacement that goes to the other components of the mechanical system. The amount of applied displacement that goes to the sample is defined as the actual displacement. In order to run the experiment, hAM samples were placed in the clamps as shown in Figure 16B. A ruler was placed next to the sample to measure the sample length before and after stretching as in Figure 16A. The actual displacement was calculated as the clamp position after stretching minus its position before stretching. The experiment process is shown in Figure 16B. Each hAM sample was stretched with 6 applied displacements: 0.05cm, 0.1cm, 0.15cm, 0.2cm, 0.25cm and 0.3cm. The max displacement, 0.3cm, is less than one full revolution of the stepper motor drive shaft, so the wire will not over lap on the shaft, and the rotation of the motor shaft is then directly related to the displacement. Two samples were used for each bioreactor channel, and each sample was used for the experiment twice.

A.   **B.**
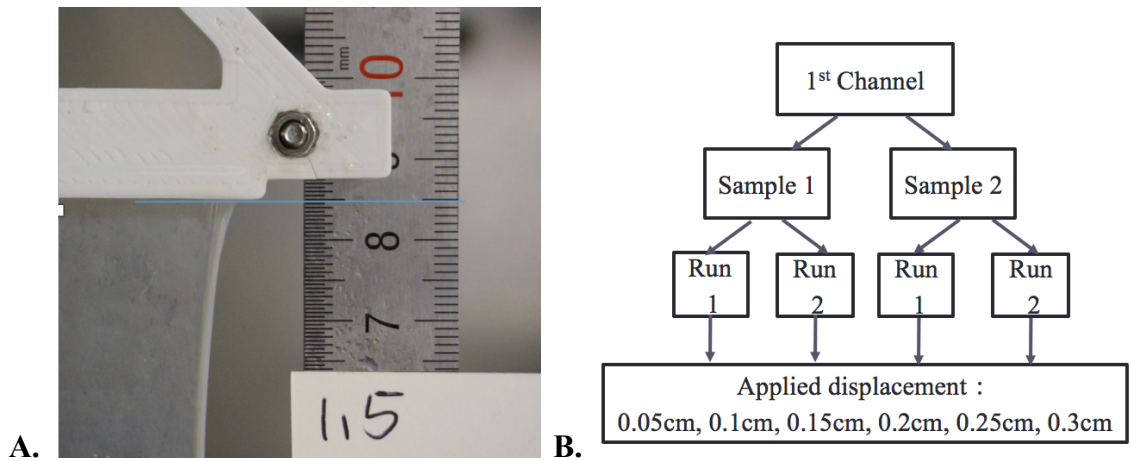
Figure 16. The actual displacement experimental setup.

A: Sample length measurement. B: Experiment process with Channel 1 as an example. Two samples are used for each channel, and each sample run the experiment twice with the applied displacement of 0.05 cm, 0.1 cm, 0.15cm, 0.2 cm, 0.25 cm and 0.3 cm.

2.1.5   *Medium Circulation System*

The medium circulation system was designed for two purposes; circulating and mixing the medium as well as changing the medium. As shown in Figure 17, the medium circulation system was composed of two parts, the part in the bio-hood and the part in the incubator. The part of the media circulation system in the incubator was designed to run continually in order to circulate and mix medium. The part in the bio-hood was only used when changing the medium, and the medium can be changed without exposure to non-sterile air. The chance of contamination while changing medium was reduced with this medium circulation system.
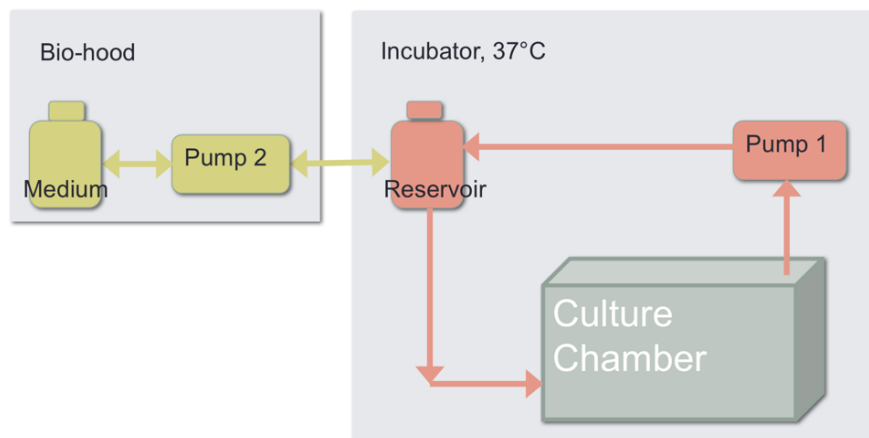
Figure 17. Sketch of the Medium Circulation System.
Pump 1 in the incubator was run constantly in order to circulate and mix medium. Pump 2 in the bio-hood was only used when changing the medium. Pump 2 is operated to first suck out the old medium into an empty bottle, and then push the fresh medium into the reservoir in the incubator.

2.1.6 Electronics of the bioreactor

2.1.6.1 Arduino Board

Arduino is an open-source physical computing platform that can take input from the sensor (i.e. load cell) and control physical output (i.e. stepper motor). Arduino is based on a simple microcontroller board (Arduino UNO board), and a development environment (i.e. LabVIEW and Arduino software) for writing software for the board. Figure 18 shows a picture of an Arduino Uno board. The USB plug is used to connect to the computer. The digital pins connect the stepper motor and an analog pin connects the load cell. In this study, LabVIEW was chosen as the programming software, and more information will be discussed in Chapter 3. Each channel of the bioreactor has one Arduino UNO board; thus four Arduino boards were used for the whole bioreactor system.

Digital I/O Pins (2-13)

USB Plug
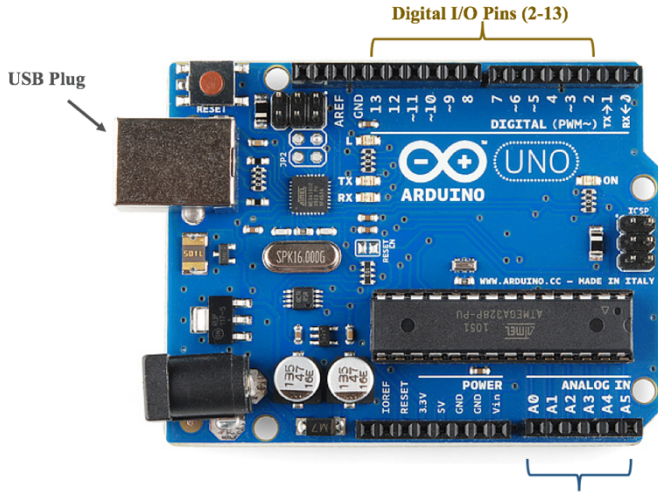
Analog In Pins (0-5) **Figure 18. Ardino Uno Board.**

2.1.6.2 Stepper Motor

The stepper motor (SM-42BYG011-25, SparkFun® Electronics, Colorado, US) was chosen because it can move by steps (1.8 degree per step) and can reach the desired movement precisely. A motor driver, EasyDriver (A3967, Allegro™, Worcester, Massachusetts, USA), was used to control the moving steps. EasyDriver is a simple to use stepper motor driver, and was linked to an Arduino control board, which connected to a desktop computer through a USB interface. A 5-volt power supply (HZPW-9V650, SunFounder, Buckinghamshire, United Kingdom) was used to power the stepper motor.
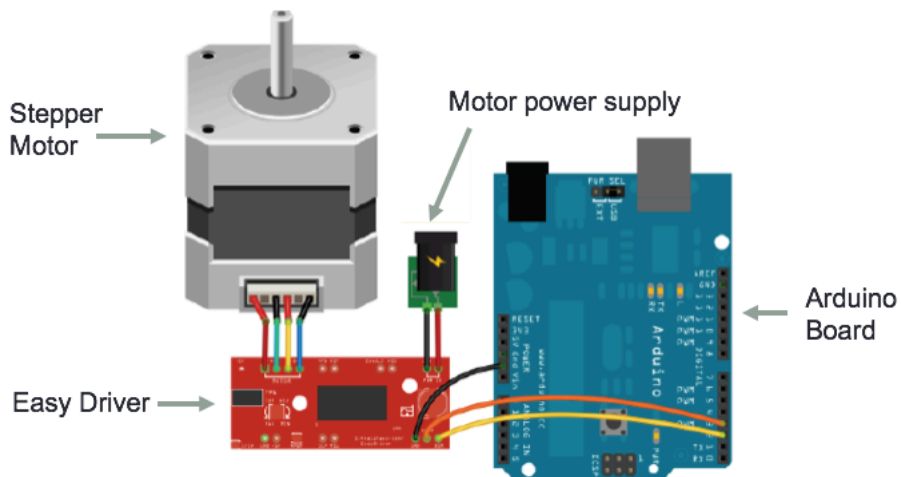
Figure 19. The scheme of stepper motor and Arduino board connection.

34

The scheme of the stepper motor, motor driver and Arduino board is shown in Figure 19. The LabVIEW program converted and transferred the user supplied moving parameters to the Arduino and then the Arduino transferred a digital signal to the motor driver, which directed the stepper motor movement.

2.1.6.3 Load cell and calibration

A load cell (0-5kg, CZL635, Phidgets, Calgary, Canada) was used to measure the force added to the tissue samples. It was connected to the pulley with a screw as shown in Figure 10. A load cell is a transducer that is used to create an electrical signal, and the magnitude of the signal is directly proportional to the measured force. The load cells used in this bioreactor system are strain gauge load cells. The strain gauge, which is a planar resistor, deforms when the material of the load cell deforms. The deformation of the strain gauge causes the change of its electrical resistance proportionally, and the resistance change provides an electrical signal value change. The electrical signal output of the load cell is on the order of a few millivolts, thus an INA125 instrumentation amplifier (Burr-Brown®, Arizona) was used to amplify the voltage to make it large enough for the Arduino board to detect. Figure 20 shows the sketch of load cell, amplifier, and Arduino board connection. A resistor was used with INA125 to control the gain, which is the extent to which the voltage is amplified. According to the INA 125 datasheet, the amount of gain is inversely proportional to the size of the resistor. The Arduino board can read voltage between 0 to 5 volts. It was important to make sure that the voltage corresponding to the maximum force required for experiments did not exceed 5 volts. After running the

35

load cell with different size resistors (from 10-ohm to 128-ohm), it was determined that a 47-ohm resistor was the best fit for this bioreactor system.
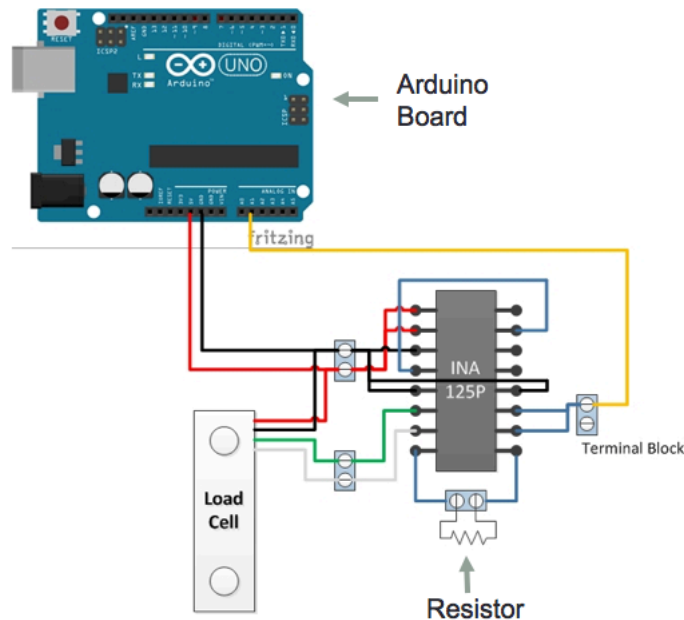
Figure 20. The sketch of load cell and Arduino board connection.

Calibration of the load cells needs to be performed to find the relationship between force and voltage before running experiments. A load cell calibration program was also written to record the voltage corresponding to the known force. 12 different weights ranging from 0 to 120 grams were used. The voltage was recorded four times and averaged for each weight. A force verse voltage graph was then made to obtain the required calibration curve.

2.2 Results and Discussion

2.2.1 Bioreactor Components

The bioreactor frame is shown in Figure 21. Arduino boards were placed outside the incubator, and the bioreactor body frame was placed inside the incubator. Load cells were fixed on to the top of the frame with the custom made brackets, and the stepper motors

were fixed to the bottom frame with a mounting bracket. Pulleys were attached to the load cells with screws. The stepper motor was connected to the sample clamps through the pulley with stainless steel wire. Stainless steel was chosen because it is strong and not easily stretched compared to other string material.
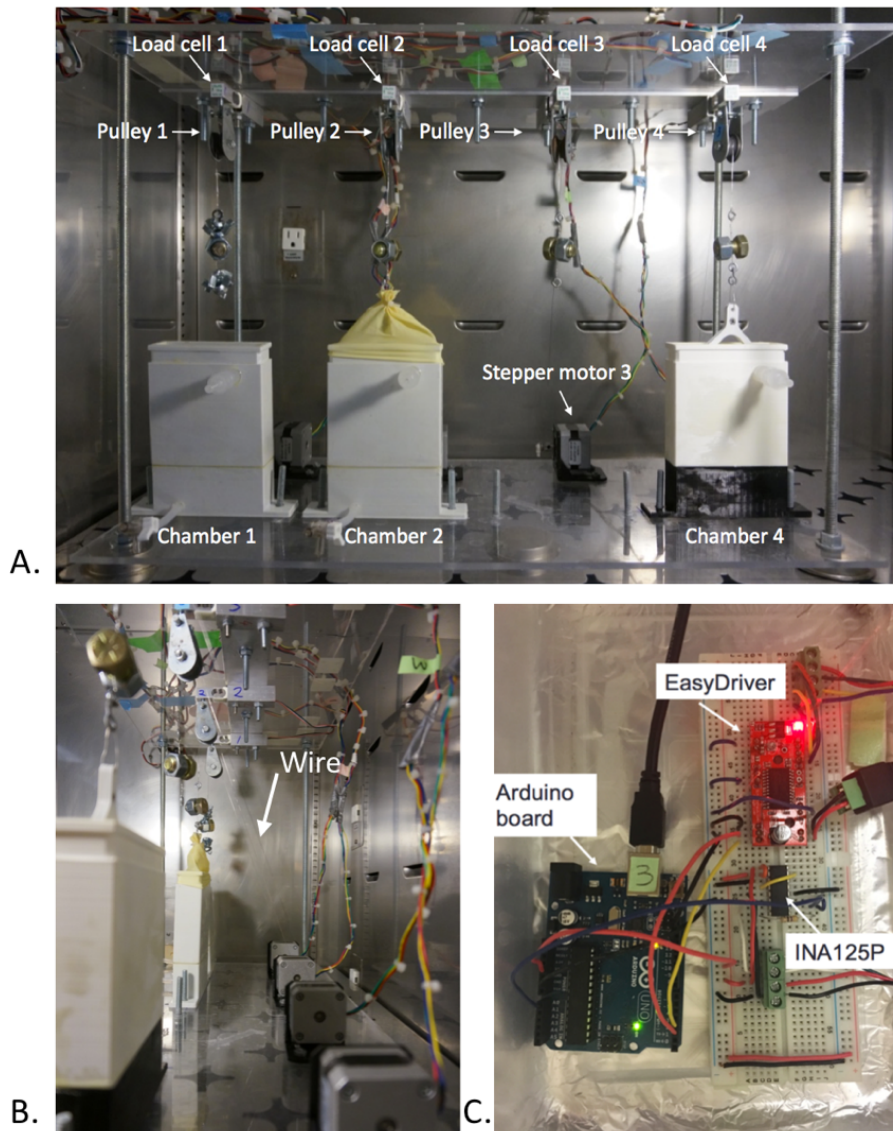
Figure 21. Bioreactor overview
A. Front view B. Side view
C. Arduino board connecting to easy driver and INA 125P amplifier.

The purpose of the actual displacement study was to find out how much the connection parts (string, clams and hook) were being stretched when stretching the hAM samples. The experiments were done for all four bioreactor channels, and they have very similar results. Channel 3 data are shown in Figure 22 as representative results. The actual displacement and the applied displacement are as defined in section 2.1.4. The displacement curve obtained from the linear least squares fit of the data for channel 3 is:

$$\text{Actual displacement} = 0.9552 \times \text{applied displacement} - 0.0527$$
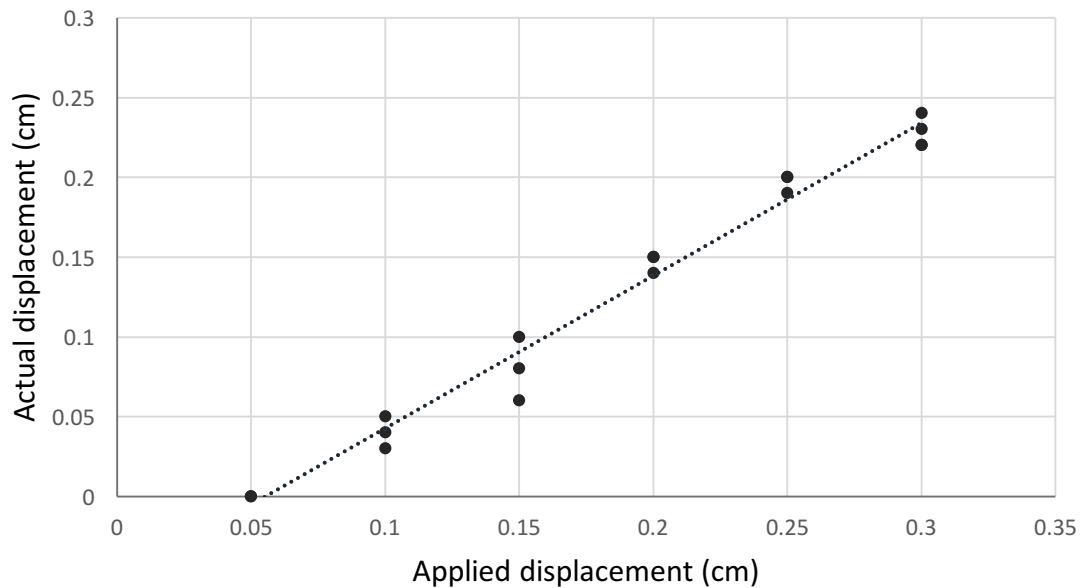
Figure 22. Experimental results of the actual displacement for channel 3. (Actual displacement $= 0.9552 \times$ applied displacement $- 0.0527$, $R^2 = 0.98$)

38

The data for the other three channels are:
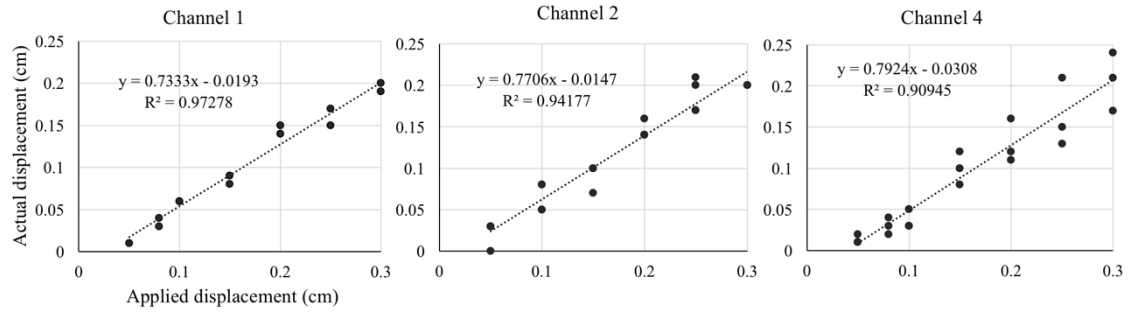
Figure 23. Experimental results of the actual displacement for channel 1,2 and 4

In order to study the accuracy of the calibration curve as a function of the applied displacement, a graph of percent difference versus applied displacement was plotted as shown in Figure 24. Percent difference was calculated as: % difference = $\frac{|Actual\ displacement - displacement\ from\ equation|}{Applied\ displacement}$. The applied displacement is the distance the motor shaft rotates, the actual displacement is the distance the tissue sample moves, and the displacement from equation is the displacement based on the equation. The difference between the actual displacement and the equation predicted displacement is less than 8% for imposed displacements greater than 0.1 cm. The percent difference curve for the other three channels shows similar result that the higher the displacement, the closer the actual displacement data fits the correlation curve.
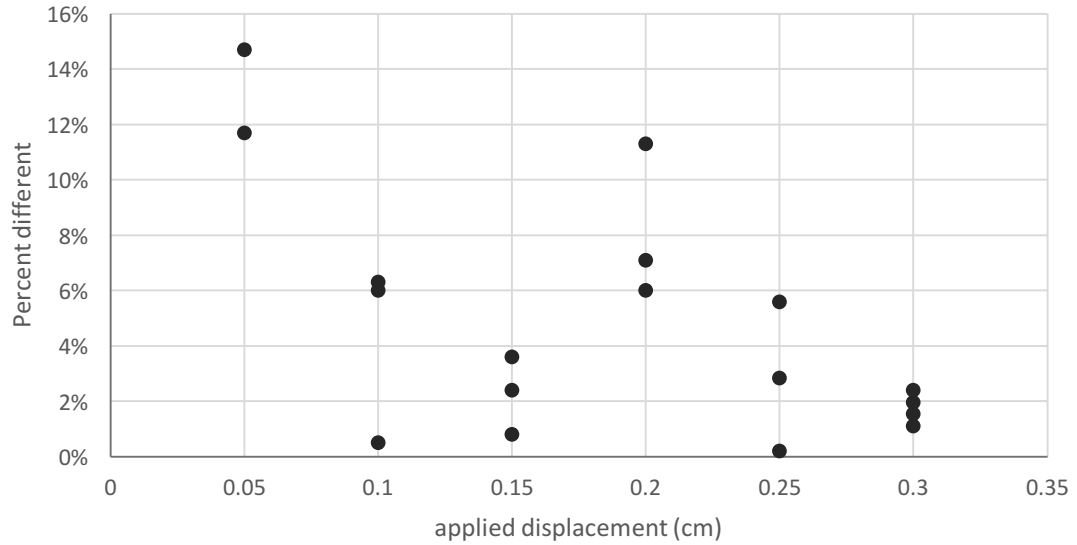
Figure 24. Percent difference verse actual displacement graph for channel 3.
Two samples were used, and the experiment was performed twice for each sample.

2.2.3   Load cell calibration

The purpose of calibration was to find out the correlation between force and voltage. All four load cells require calibration due to individual differences. The graph of force as a function of voltage was generated after testing the load cell with 14 different weights. Figure 25 shows the data of load cell 3, the calibration curve was: Force $(g) = 657.94 \times$ Voltage $(V) - 45.187$, with the R-Square value to be 0.918.

As we can see, not the all the data points were in the linear range, and the linear range started when mass of the weight was 45 g. The other three load cells had a similar shaped curve, and their linear range started when the weight were 75 g (load cell 1), 42 g (load cell 2), and 50 g (load cell 4).
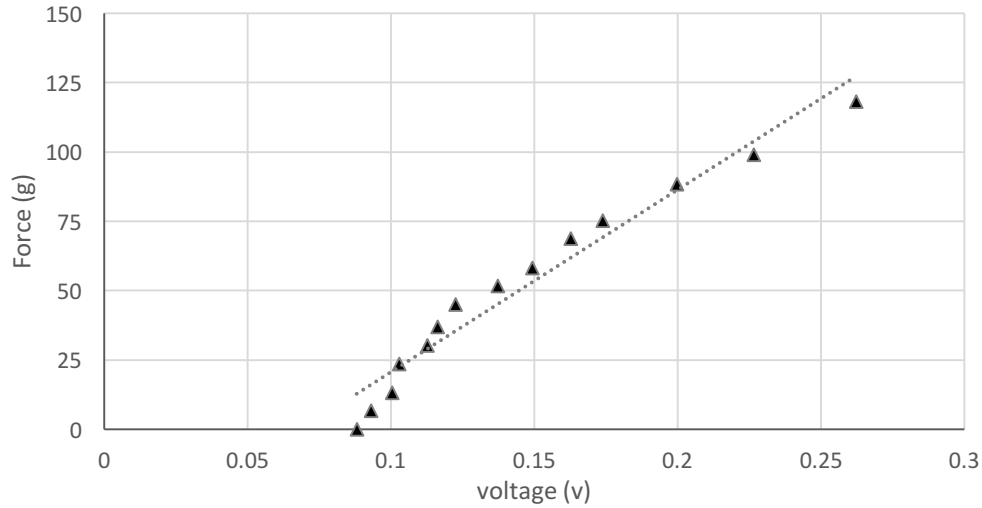
Figure 25. Load cell calibration graph: Force vs. voltage

In order to have a calibration curve that have all weight in the linear range, a 50-gram weight was added onto the wire of set two, three and four, and a 75-gram weight was added to set one to give the load cell an initial force. The load cell setup before adding the weight is shown in Figure 26A and the setup after adding the weight is shown as Figure 26B.

A.   B.
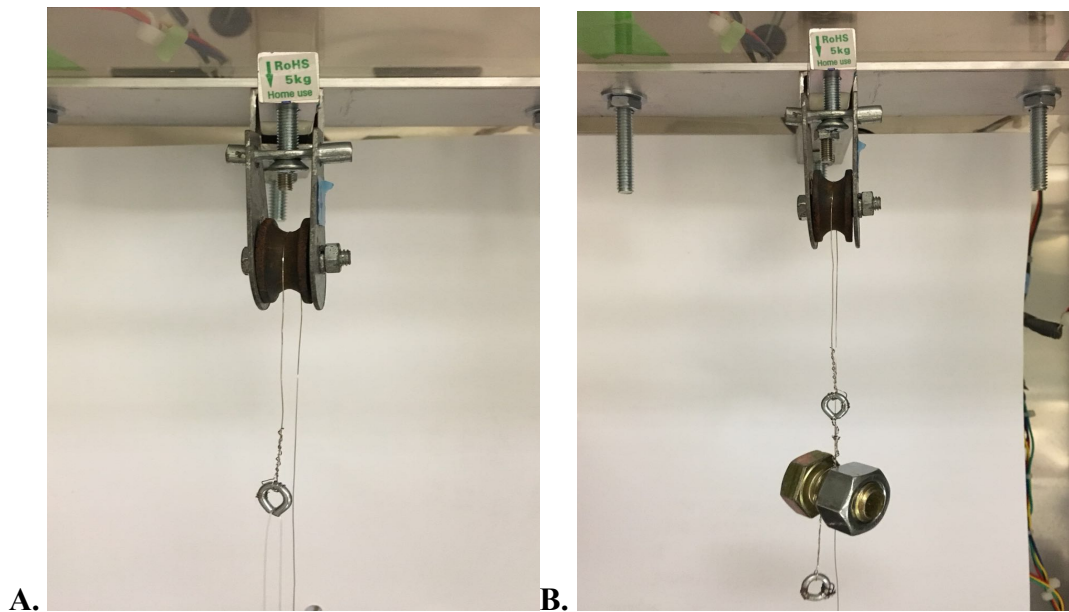
Figure 26. Load cell set up before and after add a weight

After adding an extra weight, four load cells were recalibrated with 12 different weights range from 0 gram to 120 grams. The result of load cell 3 is shown in Figure 27. Thus the adjusted calibration curve became:

$$\text{Force (g)} = 466.68 \times \text{Voltage (V)} - 50.108$$

With the R-Square value to be 0.988, it shows the points are very closely fit in the linear equation.
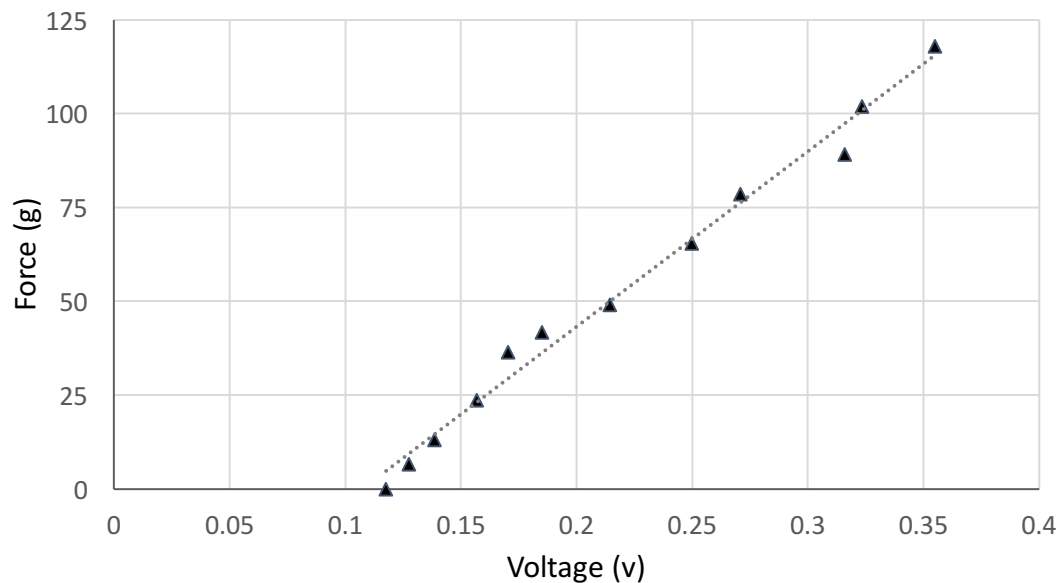
Figure 27. Load cell 3 (adjusted) calibration graph: Force vs. voltage

The voltage data in the graph is the average of four voltage reading.

The other three load cell calibration curve module are:

$\text{Force(g)} = 726.53 \times \text{Voltage-28.414 (V)}$ $R^2 = 0.958$ (Load cell 1)

$\text{Force(g)} = 449.08 \times \text{Voltage} - 64.504 \text{ (V)}$ $R^2 = 0.9881$ (Load cell 2)

$\text{Force(g)} = 444.81 \times \text{Voltage} - 39.149 \text{ (V)}$ $R^2 = 0.975$ (Load cell 4)

In order to study the accuracy of the calibration curve, the percent difference value between the recorded voltage and the theoretical voltage obtained from the calibration

curve has been determined. The theoretical voltage was calculated by plugging the known force back to the calibration. Percent difference was calculated as: % difference = $\frac{|\text{Recorded voltage} - \text{theoretical voltage from the calibration curve}|}{\text{Recorded voltage}}$. The graph of percent difference versus force of all four load cells was plotted in order to study the accuracy of the calibration curve, shown in Figure 28. Most of the data points are below 8% and the highest percent difference is 9% different, except for the one data point that is 12.5%.
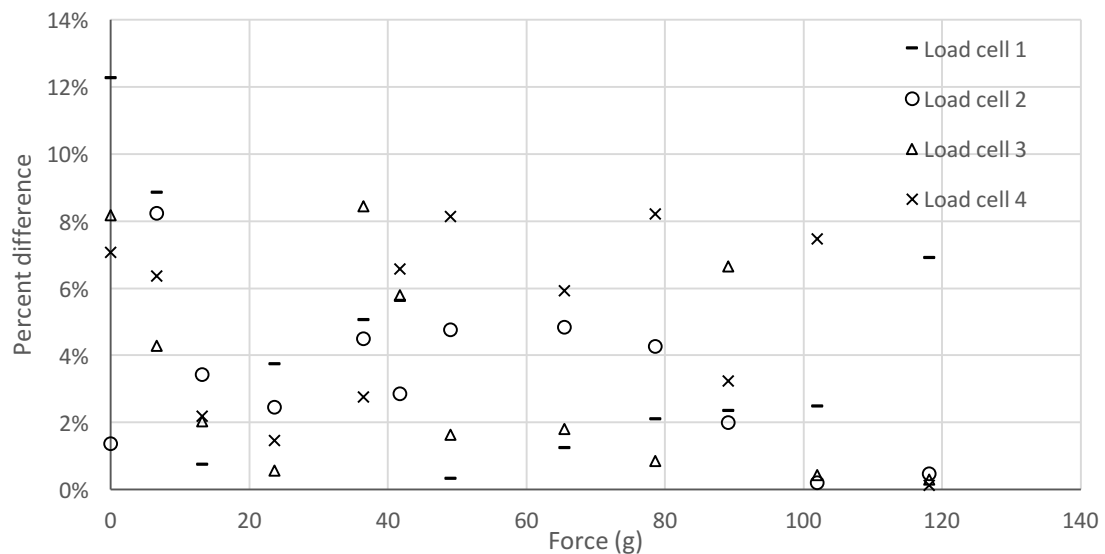
Figure 28. Percent different versus Force (g) graph of all four load cells

In order to test the consistency of the load cell calibration curve, the calibration test was repeated twice for all four load cells about a month apart. The two repeat tests were done on the same day to avoid result contingency. The calibration result of load cell 3 is shown in Figure 29 as an example. From the graph we can see that the repeat tests result was really close to each other, and were about 10 grams lower compared to the original calibration result. Similar results were observed from the other 3 load cells as well, with a 10 to 20-gram force different at the same voltage between the original calibration and the two repeated tests.
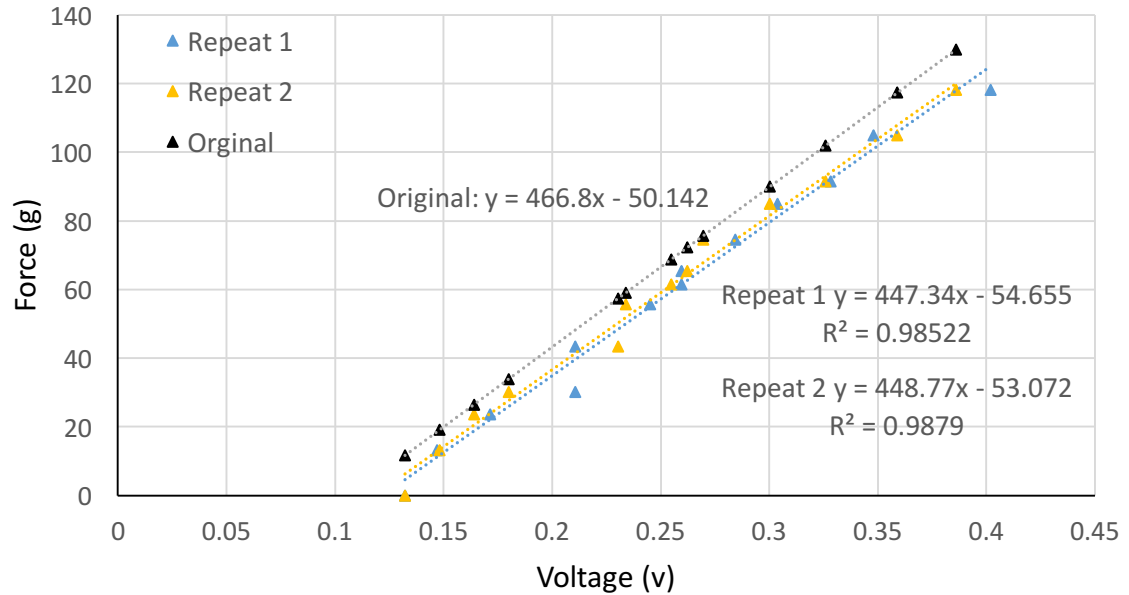
Figure 29. Repeated calibration experiments and the origianal result comparison of load cell 3

Since all four load cell repeated tests shows similar test result, it was suggested that the change could cause by external factor such as room temperature. It is suggested to calibrate the load cells before use every time. The calibration process for one load cell took about 15 to 20 minutes to perform.

2.3 Conclusion

In conclusion, the tissue sample was connected to the stepper motor with a stainless steel wire through a pulley. The stretching of the tissue sample was accomplished by the rotation of the stepper motor, and the force change was monitored by the load cell. In order to have tunable cyclic mechanical stimulation, either based on force or strain, programs are needed to control the motion of the stepper motor. The programing method and logic will be discussed in Chapter 3.

3. STRAIN AND FORCE BASED PROGRAM

As described in chapter 2, the stepper motor and the load cell provided mechanical stimulation and force monitoring for the bioreactor system. In order to achieve a tunable cyclic mechanical stimulation, custom written programs must be developed to control the stretching parameters. As mentioned in section 1.3, the current custom made bioreactors from other investigators provide either strain based stretching or force based stretching, with or without a monitoring system with it. The goal of this study is to design a bioreactor system to provide constant strain stretching with a force monitoring system, and a constant force stretching which includes a feedback system. The strain based program can also be used to study the force corresponding to a certain displacement or strain. If permanent deformation of the tissue samples occurs due to mechanical stretching, the displacement input to the strain based program will no longer provide the same strain, since the sample length has changed. Thus the force based program gives another mechanical stimulation option. In addition to that, a pre-stretch program was also developed to help locate the tissue sample at a desired initial position, and improve the consistency for the experiments.

3.1 Material and Method

3.1.1   LabVIEW

LabVIEW, which stands for Laboratory Virtual Instrument Engineering Workbench, is a system-design platform and development environment for the graphical language G. The graphical language G is a dataflow programming language, and it is different than traditional programming languages C, C++, and Java. The traditional languages program

with text, but language G can create a program with graphical notation, which makes the engineering systems easier to visualize, create, and code[66]. LabVIEW programs are called virtual instruments (VI). When a VI is created, two windows appear, a front panel window and a block diagram window. Front panel is the user interface and block diagram is equivalent to program code. The front panel consists of controls and indicators. The controls are input, which allow the user to provide information to the VI. The indicators are outputs, they indicate and display the result based on the input given to the VI. Visual Package Manager (VIPM) software was used to manage LabVIEW add-ons, such as the LabVIEW Interface for Arduino (LIFA). LIFA is the tool kit that connects Arduino with LabVIEW, and it includes some sub-virtual instruments (sub-VIs) designed for electronic devices including the stepper motor. A sub-VI is equivalent to a subprogram. These sub VI's have codes already written, which makes it easier to write programs with LabVIEW. Some of the main sub-VIs used in this study are shown in Table 3 below. "Arduino Init" initialized the connection between LabVIEW and Arduino board, and "Arduino Close" ends the active connection. "Arduino stepper configure" specifies the digital pins for stepper motor drivers. As mentioned Chapter 2.1.6.1 and Figure 17, the Arduino Uno board has 11 digital pins and 5 analog pins. The stepper motor driver connects to two digital pins and the load cell connects to one analog pin. Thus, which two pins are being used needs to be known by the program. "Arduino stepper write" specifies the motor moving steps and speed. "Arduino stepper ToGo" and "Arduino Stepper Wait till Steps to complete" monitors and adjusts the motor movement. "Stepper close" stops the motor movement. "Arduino Analog Read Pin" is used to read the voltage change from the load cell. VISA resources (Virtual Instrument Software Architecture resource) are the

46

instruments in the system. Arduino boards are the instruments in this four channel bioreactor system. Each board is considered as a VISA resource, and is named as COM 1 to 4. The "VISA resource" sub-VI defines which Arduino board is connected to the system.

Table 3. Description of the main sub-Vis

Sub-Vis	Name	Description
	Arduino Init	Initialized a connection to an Arduino running the LabVIEW interface for Arduino sketch
	Arduino Close	Closes the active connection to an Arduino
	Arduino Stepper Configure	Specify the digital pins for stepper drivers
	Arduino Stepper Write	Specify the speed and number of steps to move the stepper motor
	Arduino Stepper ToGo	Check to see if the Arduino is still processing a previous step command to ensure step commands are not overwritten
	Arduino Stepper Wait Till Steps Complete	Allows execution to continue after there are no further stepper commands in need of processing
	Arduino Stepper Close	Sets stepper control pins to low
	Arduino Analog Read Pin	Reads the analog voltage on the selected Arduino analog input (A0-A5)
	VISA resource	Define with instrument is connected to the system

The stepper motor block diagram, which is the program code, is shown in Figure 30A. Arduino Init initiates the connection between the program and Arduino board. The "VISA resource" sub-VI controls which Arduino board is connected. The digital pin number 2 and 3 on the Arduino are used to connect to the easy driver. The number of steps to move is a control, and the steps value will be input by the user. The stepper motor rotate speed

is set to be 10 steps per second. An indicator is attached to the Stepper Write VI that

allows for the motor rotate speed to be shown on the front panel. The "steps remaining?"

is an indicator of the stepper motor condition, and tells if it is running or stopped. The

front panel of the stepper motor VI is shown in Figure 30B. "VISA resource" and "# of

steps to move" are controls, which require input from the user. "Steps remaining?" light

indicates the stepper motor condition. The stop button can stop the program at any time.

A.

B.
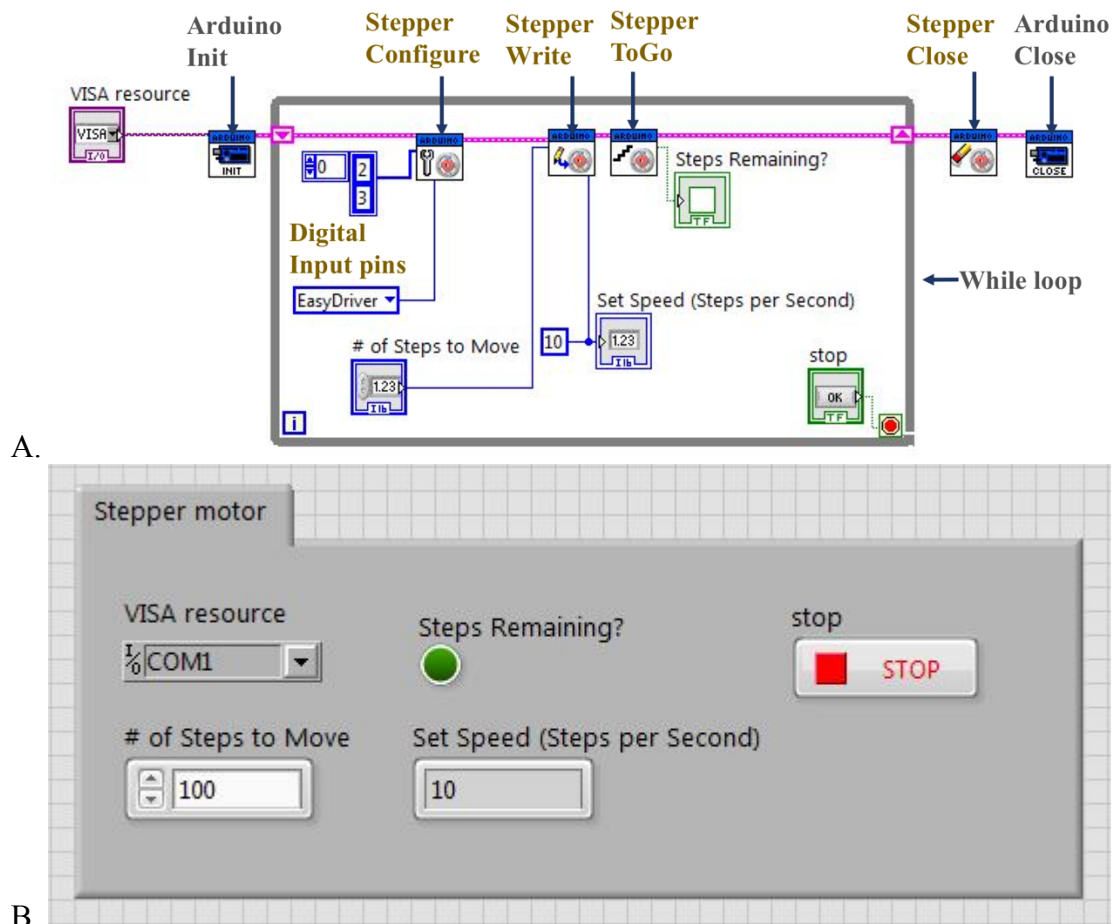
Figure 30. An example stepper motor program
A: Block diagram. "VISA resource" is a control, and the user can choose which Arduino board to connect to system. "stepper configure" initiates the motor, and the easy driver is connected to Arduino board through digital pin 2 and 3.; "stepper write" controls the motor moving steps and speed, the steps is set to be 10 steps per second; "stepper to go" monitors the motor movement, and "stepper close" stops the motor movement. The "Arduino close" end the active Arduino connection. B: front panel. "VISA resource" "# of steps to move" and "stop" are controls need input from user. "Steps remaining?" and "Set speed" are indicators.

48

3.1.2   Parameter definitions and logic for the programs

The goal of this project is to have a tunable program to control the stretching parameters including percent strain, move time, relax time, and number of runs, stretching time, and hold time. Percent strain is the stretched distance over the original sample length. The definition of time related parameters are explained in Figure 31. A single run consisted of a moving time period and a relax time period (Figure 31A). Moving time represents the time period that the tissue sample is being stretched. Relax time means that the sample is motionless, and there is no extra force added to it. During the moving time, the tissue sample was being stretched and released. As shown in Figure 30B, stretching time was the time the sample takes to reach the desired strain. Hold time 1 represents the time period that the sample stays at the stretching position. Release time is how long it takes for the sample to go back to the original position. Hold time 2 stands for the waiting time before next stretch starts. A single stretch loop of the tissue sample movement is stretch, hold, release, and hold. Multiple stretch loops happen during the move time, the number of loops depends on the moving time and the time it takes to run a single loop.
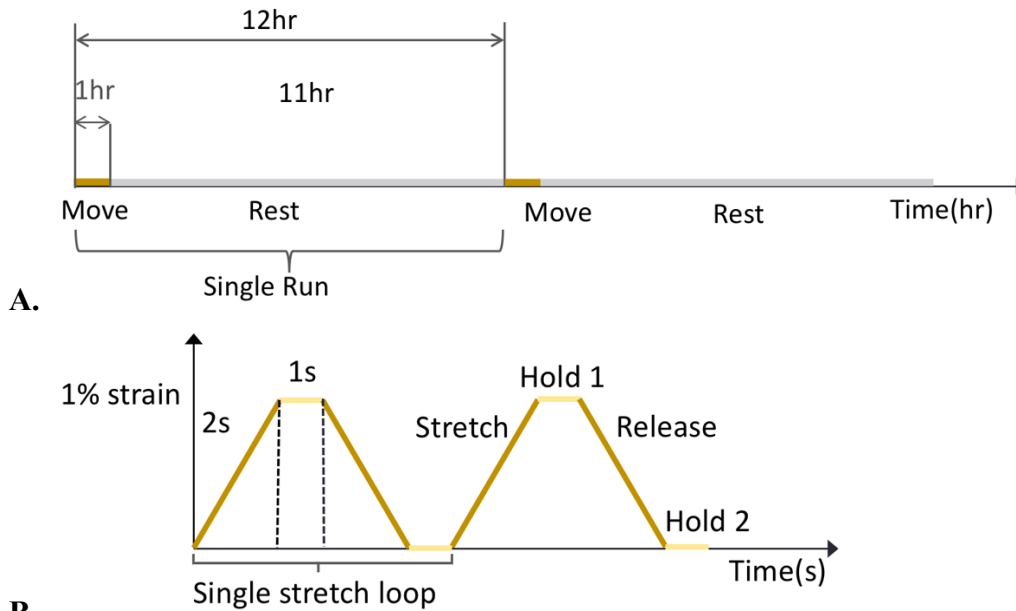
Figure 31. Mechanical stimulation related parameters definations
The example of single run shown in 31A consisted of 1 hour move time and 11 hour relax time. 31B illustrated a single stretch loop movement with an example of 1 % strain: stretch the sample for 2s, hold for 1s, release for 2s, and hold for another 1s. Another loop of stretching was continued after.

Based on the bioreactor design criteria and mechanical stimulation parameters, a basic program logic was developed, as shown in Figure 32. The load cell and stepper motor were connected to the Arduino board separately though analog pins and digital pins. The Arduino received analog signals from the load cell, and provided voltage data to the LabVIEW software. The voltage data was then converted to force data through the calibration curves, as discussed in section 2.2.3. Mechanical stimulations are accomplished by the rotation of stepper motor shaft, which was controlled through digital signals from the Arduino board. The stepper motor control logic follows the mechanical stimulation parameters character, which include the move and rest sections. Stretch, hold 1, release, and hold 2 are included in the move section. Both constant percent strain and the constant force programs were developed based on this basic programing strategy. The

logic of load cell programing was the same for both programs, which was constantly measuring the force data. The stretch part of the stepper motor coding was different. The constant strain program provided stretching by rotating the motor shaft for a certain number of steps. The constant force program provided stretching by rotating the motor shaft until the desired force was reached. More details will be discussed in section 3.1.3 for constant strain program and 3.1.4 for constant force program.
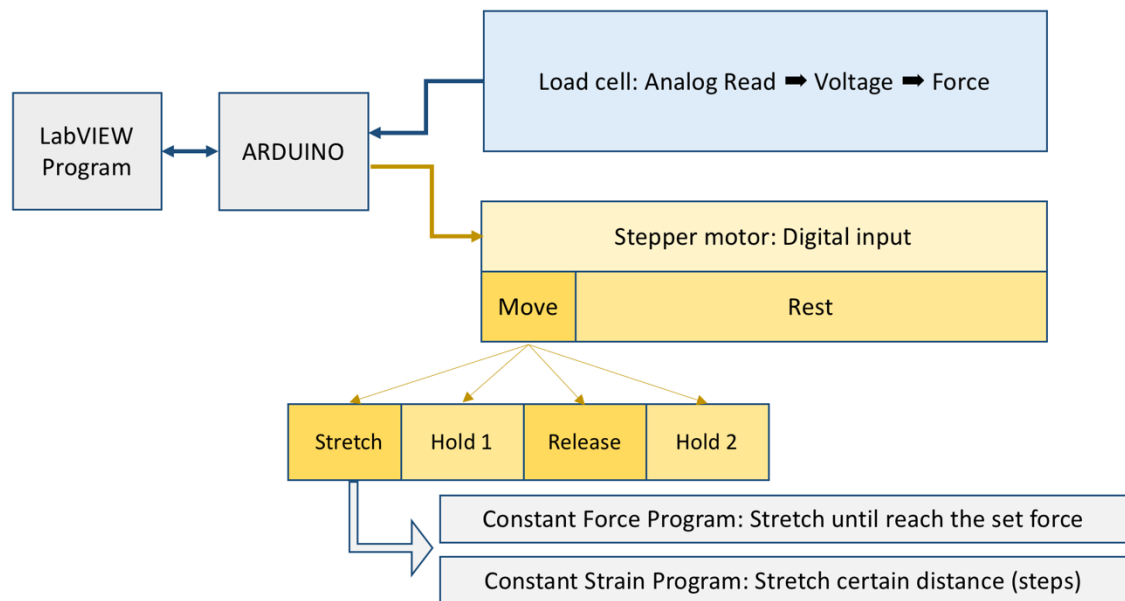
Figure 32. The basic logic of LabVIEW stretching program
Load cell connects to the Arduino board through analog pin, and provide a voltage feedback to the program through Arduino. Stepper motor connects and receives order through the Arduino board through digital pins on Arduino board. When running the constant force program, the motor shaft rotates till reach the desired force. When running the constant strain program, the motor shaft rotates a certain step.

3.1.3   Strain Based Program

The strain based program allows the tissue sample to be stretched to a certain displacement. It is relatively straight forward to accomplish with the stepper motor as long as the number of steps, i.e. the displacement of the tissue sample, is known. The logic of the constant strain program is shown is Figure 33. The load cell constantly

provides a voltage signal to the system in order to monitor the force that has been added to the tissue sample. At the same time, the stepper motor shaft rotates back and forth to provide mechanical stimulation.
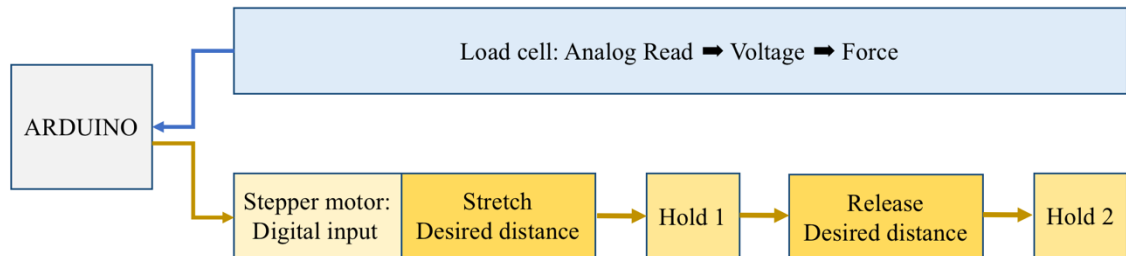
Figure 33. The design ogic of constant strain program
The load cell monitors the force change. The stepper motor shaft rotates forward to stretch the tissue sample, hold for a certain time, rotate backward to release the sample, hold for some time before the next loop starts. The number of loops is decided by the move time and the total time takes to for one loop.

The stepper motor needs to be told how many steps it needs to move. The steps can be calculated from the sample size, percent strain desired, and the diameter of the motor shaft. The displacement was the sample length multiplied by the desired percent strain. It took the stepper motor 200 steps to move one complete rotation. Thus the distance of the movement per step is based on the perimeter of the axis of rotation. Based on the displacement and distance per step of the stepper motor, the number of steps can then be calculated.

$$\text{Sample length} \times \% \text{ Strain} = \text{Displacement}$$

$$\frac{\text{Distance}}{\text{Step}} = \frac{\text{perimeter}}{\text{Steps per circumference}} = \frac{\pi d}{200}$$

$$\text{Steps to move} = \frac{\text{Displacement}}{\frac{\text{Distance}}{\text{Step}}}$$

After the number of steps was calculated, the stepper motor shaft would always rotate the same number of steps for every stretching loop during the move time.

The constant strain program includes two main block diagrams. The first one is the force monitoring block diagram, as shown in Figure 34. The "Current time" VI tells the current time. The "Arduino Analog Read" VI reads the voltage data form loadcell. The voltage data was then pluged into the calibraiton curve to get the force data. The "build graph" VI then collects the time and force data and creates a force vs. time graph to show on the user interface. At the same time, the "write to file" VI records the time and force data to an excel file. The "wait time" VI controls how often the "Arduino Analog Read" VI reads the voltage data.
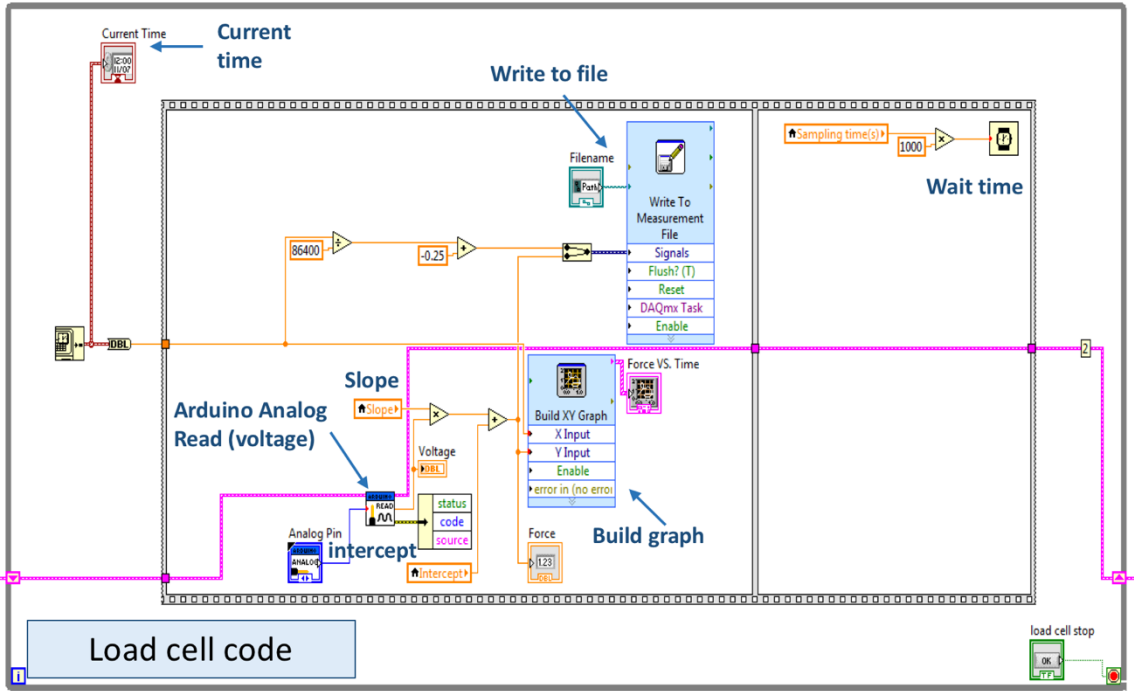
Figure 34. Load cell part of Blockdiagram for the constant strain program.
The "Current time" sub VI tells the current time. The "Arduino Analog Read" sub-VI reads the voltage data from load cell. The voltage data was then plugged into the calibration curve to get the force data. The "build graph" sub-VI collects the time and force data and create a force vs. time graph to show on the user interface. The "write to file" sub-VI record the time and force data to a selected excel file. The "wait time" sub-VI controls how often the "Arduino Analog Read" sub-VI reads the voltage data.

The second block diagram is for motor control, as shown in Figure 35. The motor control

block diagram has four parts of VI: strech, hold 1, release, and hold 2. Hold 1 and hold 2

use the "wait time" sub-VI to hold the stepper to be static for a certain time before going

to next part of VI. Both stretch and release VIs include stepper motor sub-VIs to control

the motor movement. "# of steps to move" and "Set speed" input the moving distance and

speed. The "# of steps to move" value is negative for the release VI so that the stepper

motor shaft rotates backward.
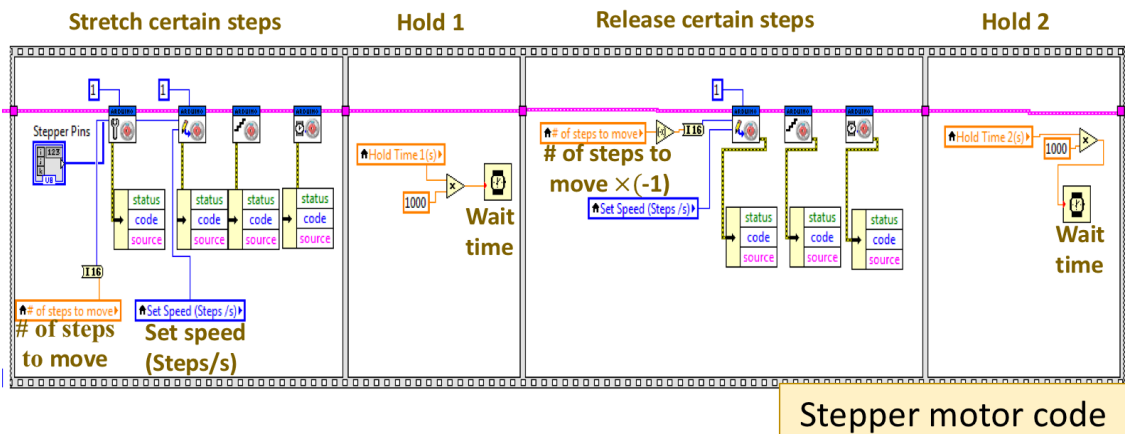
Figure 35. Block Diagram of the motor control VI for the constant strain program
Stretch and release VI include stepper motor sub-VIs to control the motor movement. "#
of steps to move" and "Set speed" control the moving distance and speed. The "# of steps
to move" value is negative for the release VI so that the stepper motor shaft rotates
backward. Hold1 and hold 2 use the "wait time" sub-VI to hold the stepper to be static
for a certain time before going to next part of VI.

The user interface of the constant strain program is shown in figure 36. The required

inputs on the parameter control page (figure 36A) are VISA resource, sample length, %

strain deisred, file name, and time related parameters, which were described in section

3.1.2. All the controls are shown in a white backgroud, and the indicators (such as current

time, displacement, force vs. time graph) are shown in a grey backgroud. The basic setup

(Figure 36B) parameters are the diameter of motor drive shaft, the slope and intercept of

54

the calibration curve, and load cell samlping time. After typing inputs for all the controls,

click the button "start" on the user interface to start running the program.

A.

B.
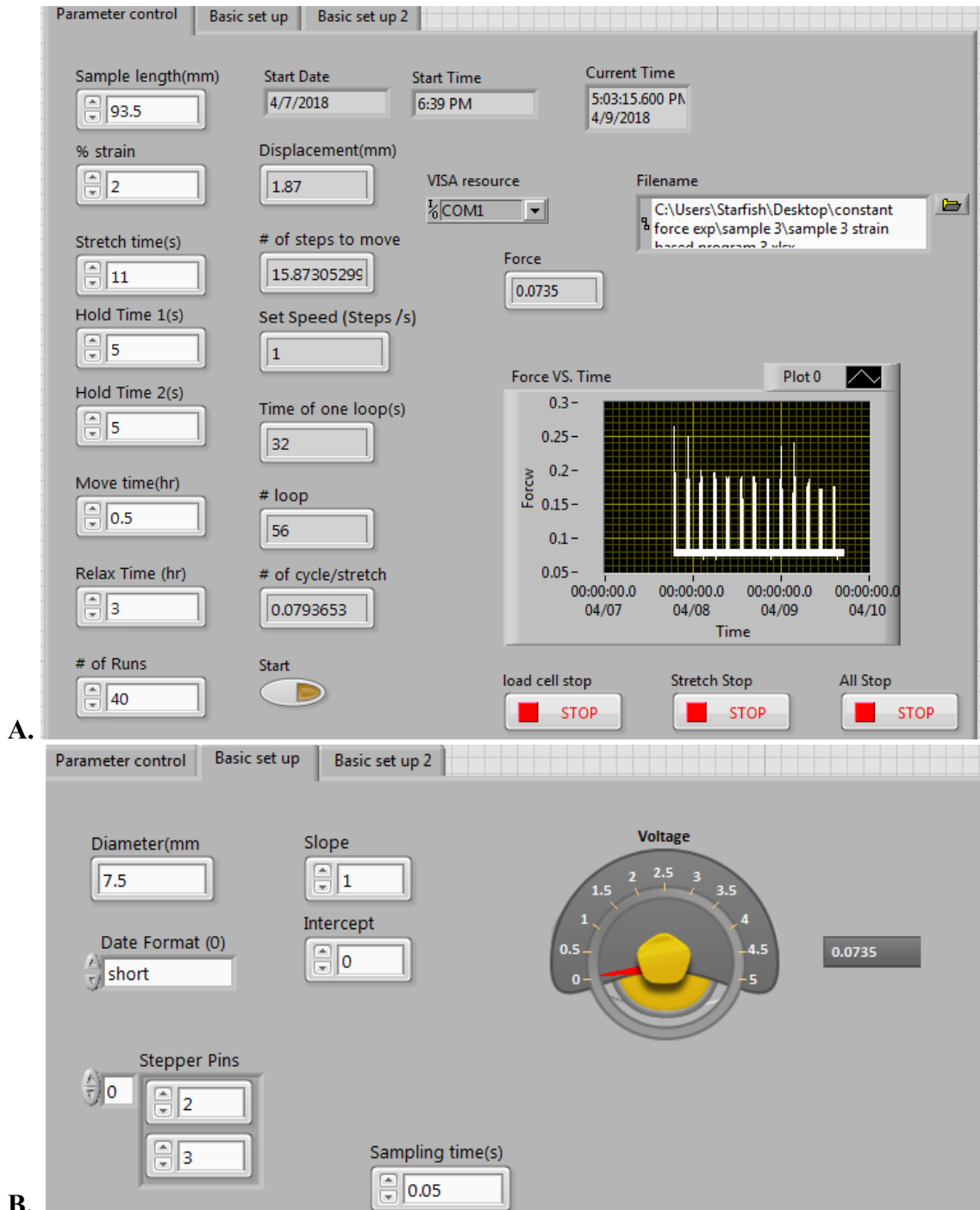
Figure 36. Constant strain program interface

A: Parameter control page B: Basic set up page. The inputs on parameter control pages determins the sample displacement and streching speed and frenqucy, as long as the number of runs.

3.1.4 Constant Force Program

While the constant strain program provides a constant distance of stretching, permanent deformation could happen to the tissue sample. If the sample gets longer because of energy loss and deformation, the actual percent strain would decrease and no longer maintain the constant strain. The constant force program stretches the tissue sample until it reaches a desired force, and then releases the tissue sample to another desired force. The maximum desired force tissue sample is stretched to is defined as "desired force top," and the force the tissue sample is allowed to relax back to is defined as "desired force bottom" The program logic is shown in Figure 37. The load cell logic is similar as the constant strain program. The force data does not affect the stepper motor movement in the constant strain program. However, the constant force program compares the instantaneous force to the desired force and controls the motor shaft movement based on the result of this comparison. If the instantaneous force is smaller than the "desired force top," then the stepper motor shaft will rotate forward to stretch the sample until it reaches the "desire force top". When the desired force has been reached, the stepper motor shaft stops turning and the program moves on to the "hold 1" stage. After "hold 1" stage, the stepper motor shaft will rotate backward to relax the sample until it reaches the "desire force bottom", and then proceeds on to the hold 2 stage.
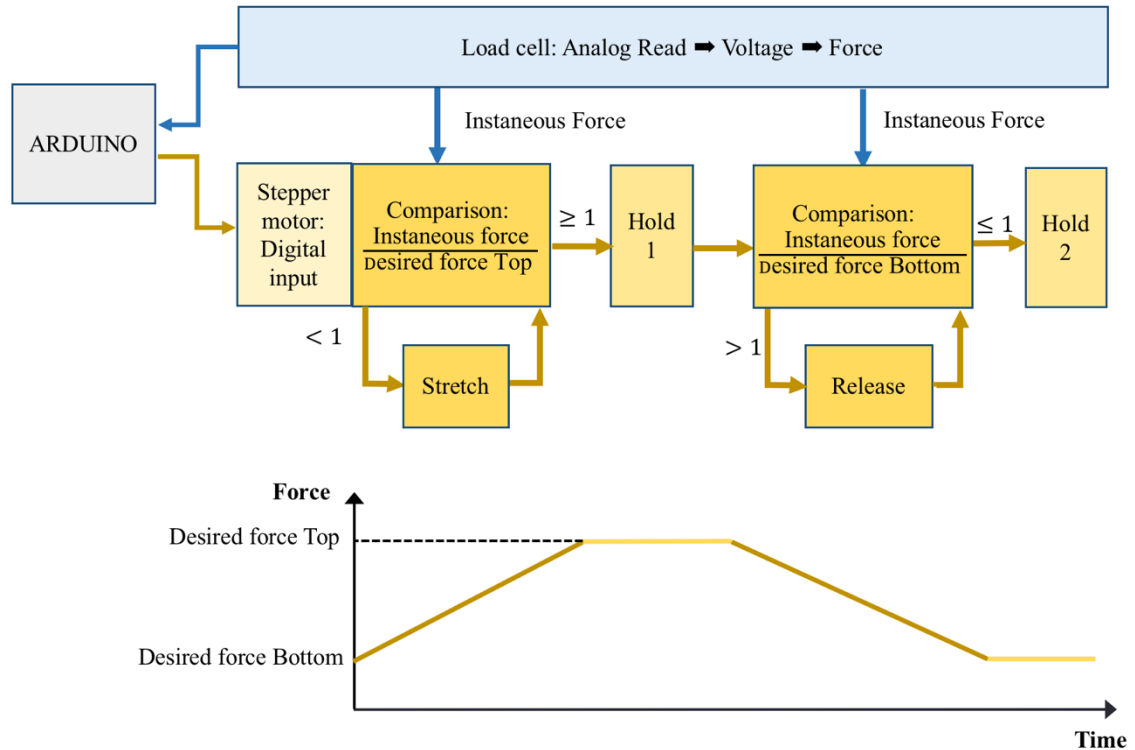
Figure 37. The design logic of the constant force program
The instaneous force feedback from the load cell is compared to the desired forces. At the stretch stage, if the instaneous force is less than the desired force top, the motor shaft rotates forward to stretch the till sample till the defired force is reached. When reach to the release stage, the motor shaft will rotate backward till the desired force bottom is reached.

The load cell block diagram is the same as in the constant strain program. Figure 38A shows the block diagram of the stretch part. The instaneous force was obtained from the load cell, and compared to the "desired force top." As long as the instantaneous force was smaller than the force needed, the case structre would be under the true condition, and the motor would continue moving until the false condition was reached. The false condition was when the instantaneous force was larger than the force needed. the second and fourth block were the same as the constant strain program, which included the code for resting. Figure 38B show the code for the relax part, which had the same logic as the streching code, but with a different desire force input.
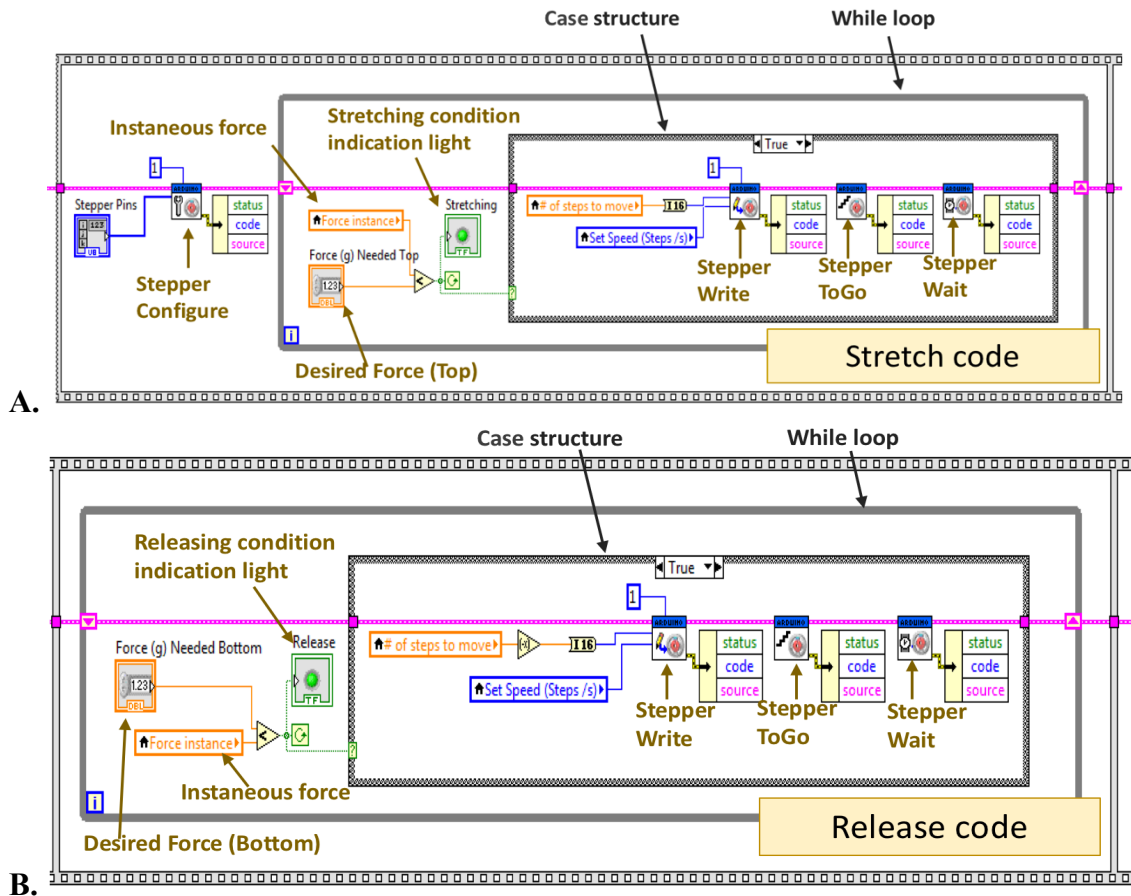
Figure 38. Stretch and release block diagram (program code) of the Constant Force Program

The user interface of constant force program is shown as Figure 39. Instead of having a percent strain input, two desired force values decided by the user are required for the program. The "Force Needed Top" is the force that the membrane needs to be stretched to. The "Force Needed Bottom" is the force to which sample is allowed to relax. After typing inputs for all the controls, click the button "start" on the user interface to start running the program.
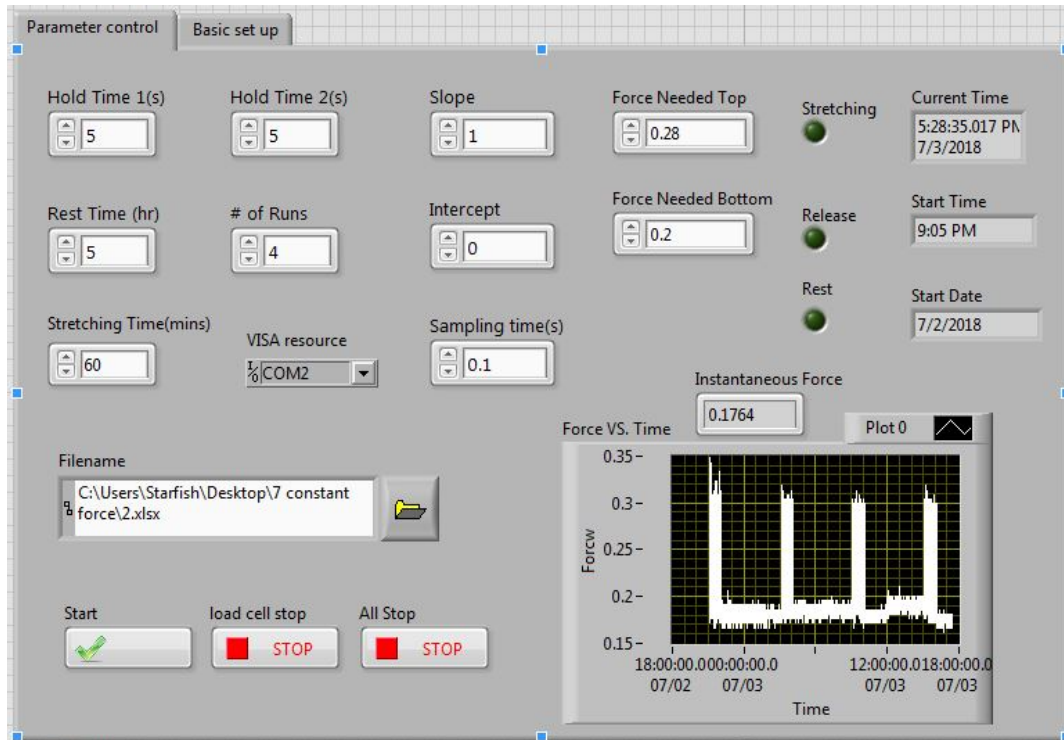
Figure 39. User interface of Constant Force Program.
VISA resource shows as COM2 indicate that channel 2 is currently connected to the program. Hold time 1 and 2 are both 5s, the stretching time is 60 minutes and rest time is 5 hours. A single run takes 6 hours, and there are four runs. The Desired force top is 0.28g and bottom 0.2g. The lights indicate with stage is running.

3.1.1 Pre-Stretch Program

The second objective of this study is to develop a program that is able to make sure the tissue samples stretch from a consistent initial position. To achieve this, the pre-stretch program was designed to have the load cell constantly measure the force on the tissue sample, and provide visual feedback to the user through a force vs. time graph. At the same time, the stepper motor shaft rotates forward and backward adjusting the tissue sample position until it reaches the desired position.

Figure 40 shows the block diagram of the pre-stretch program. The load cell coding is on the top of the block diagram. The bottom part of the block diagram controls the stepper motor shaft rotate speed and direction with a case structure. When the "stretch forward"

59

button is off, the case structure is under false condition and the stepper motor would not be moving. When the "stretch forward" button is on, the case structure is under the true condition, and the motor shaft rotates continuously. When the input of "# of steps to move" is positive, the motor shaft rotates forward; when it is negative, the motor shaft rotates backward. With this code, the stepper motor movement can be controlled by the user with the "stretch forward" button and the value of "# of steps to move" while running the program.
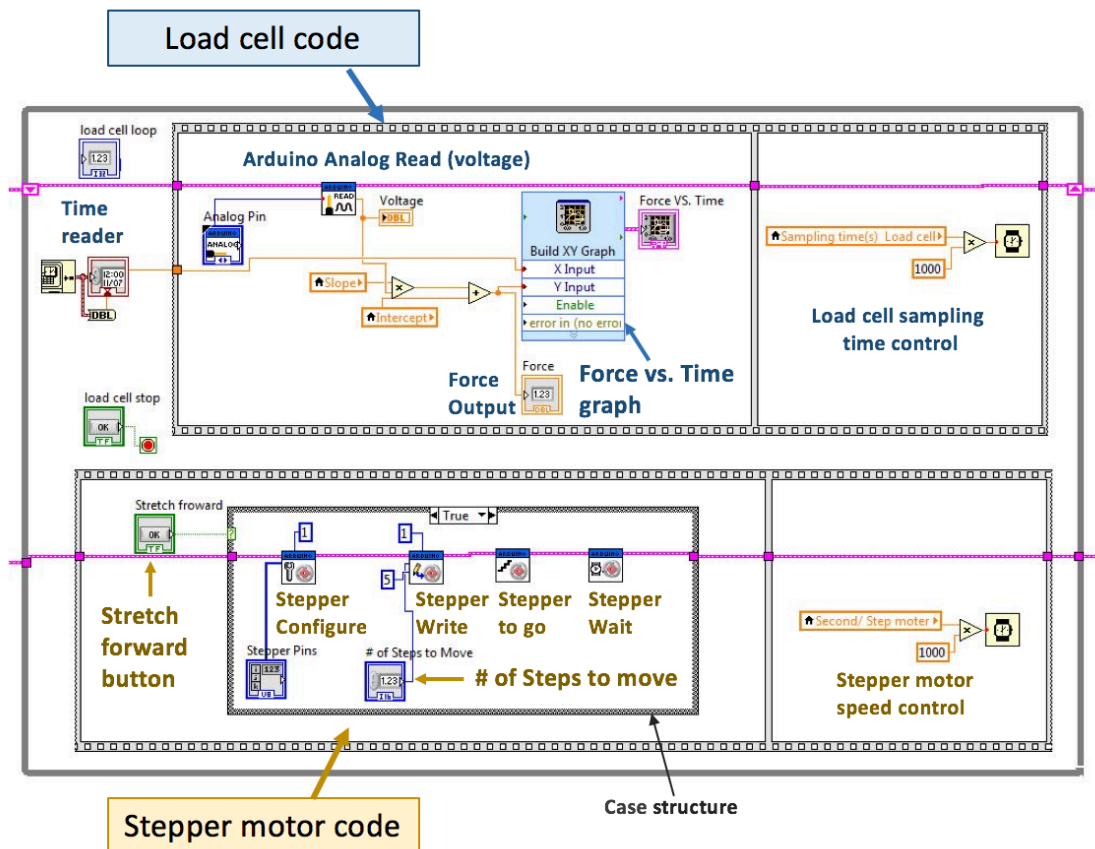
Figure 40. Block Diagram of Pre-Stretch Program

The pre-stretch program user interface is shown in Figure 41. "Load cell sampling time" "# of steps to move" and "Second/ step motor" values need to be input before running the

program. The constant strain and force programs are autonomous after the program is

initialized, but the pre-stretch program requires user action after the program is running.
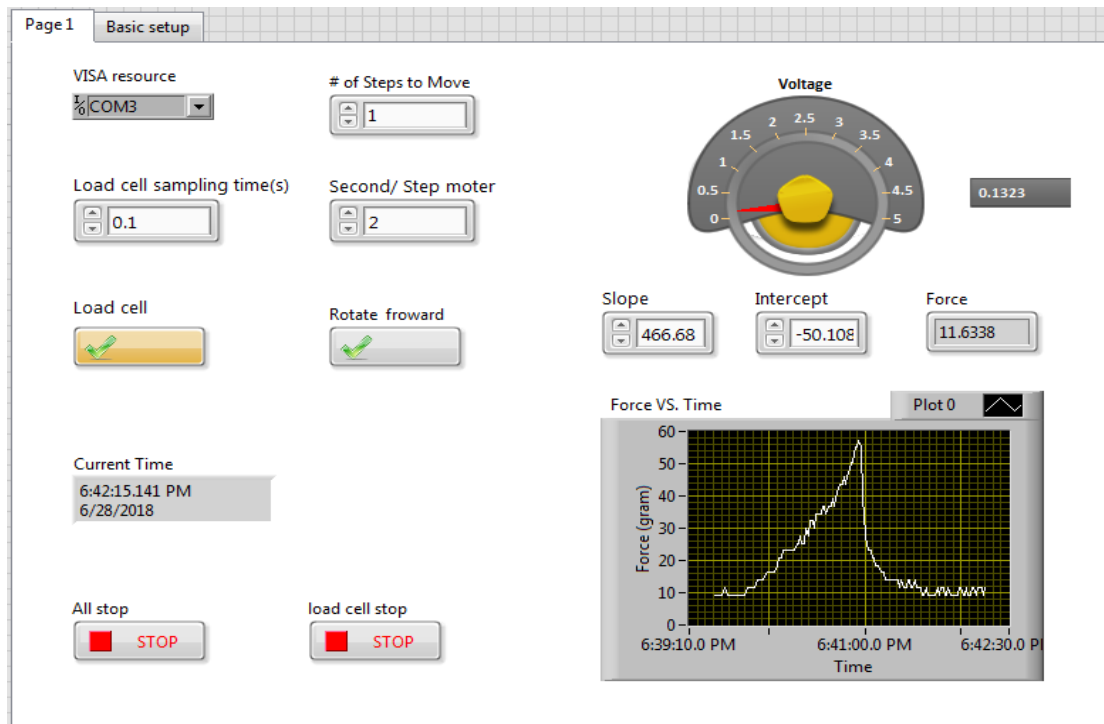
Figure 41. Front Panel of the pre-stretch program with channel 3 as an example
LabVIEW record force data every 0.1s, the stepper motor shaft rotates 1 step every 2s.
the graph record the force change. The "load cell" button is on, and the "rotate forward"
button is off in this picture.

When the "load cell" button is clicked, load cell starts measuring force. When the "stretch

forward" button is clicked, stepper motor shaft rotates forward. The force vs. time graph

is shown on the interface for users to observe the force change. By changing the "# of

steps move" value to a negative number, the motor shaft rotates backward. When the

"rotate forward" button is clicked again, it will be off as shown in Figure 42, and the

stepper motor will stop moving. When the desired position is reached, the user can end

the program by clicking the "stop" button. The whole process usually takes less than 5

minutes.

61

3.2 Result and Discussion

3.2.1　Pre-Stretch Program

With the pre-stretch program, it was possible to place the tissue sample at a desired initial position, which was decided by the user. Figure 42 gives an example of how a tissue sample reaches 0% strain position. The sample was loaded into the chamber at a relaxed position, which was less than its original length to make sure there was no extra force added to the sample at all. Then running the pre-stretch program, the load cell started measuring the force. At this time, there was no force cause by stretching added. Then click the "stretch forward button", and the stepper motor started to move step by step to start to stretch the membrane. When the force started increasing, it meant the sample was being stretched. The stretched sample started being released by reversing the motor shaft moving direction. When the force shown was equal to the original force, the motor was stopped immediately. The sample now was at a 0% strain position.
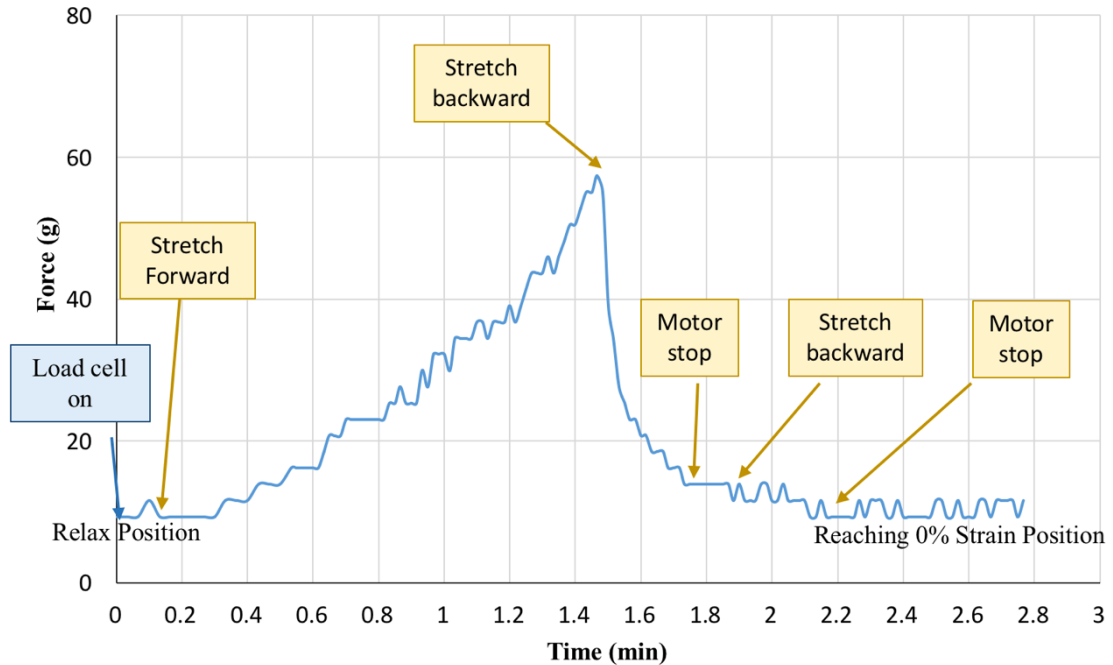
Figure 42. The sample reached at the 0% strain position with pre-stretch program
The tissue sample was at relax position when the load cell starts measuring the force. Then the motor shaft starts to move the tissue sample up. When the tissue sample is being stretched, change the moving direction to rotate backward, and the tissue sample goes to the relax stage. When the instanteous force first equals to the force at relax position, stop the motor movement immediately. At this point, the tissue sample is at 0% strain position.

3.2.2 Constant Strain Program

Two types of experiments were performed to test the constant strain program. The first experiment was a static condition, where the stepper motor was turned off and only the load cell was taking measurements of the same weight for three days. This experiment was performed to make sure the load cells were able to measure the force without drifting. The second experiment was with the stepper motor providing constant strain stretching to make sure the program was able to perform stretching as the user desires.

The first experiment was performed on all four bioreactor channels at the same time. Figure 43 shows the recorded voltage data points from load cell one, and as we can see, the voltage reading are consistent and the load cell sensitivity is high. The average voltage

was 0.147 v±0.0027, with a percent standard deviation of 1.9%. Over three days, 76,299 voltage reading were collected by the program. There were six different voltage readings in this graph: 0.1323 v, 0.1372 v, 0.1432 v, 0.147 v, 0.1519 v and 0.1568 v. The smallest detectable reading set by our equipment was found to be 0.0049v. The frequency distribution of data points is shown in Figure 44.
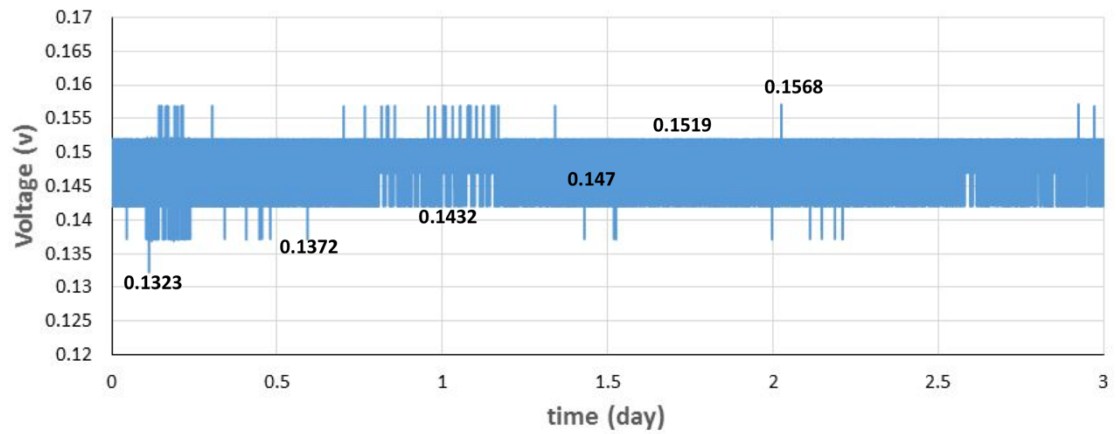
Figure 43. Constant Strain Program (0% strain) experimental result.
All 76299 data points included. Voltage is 0.147±0.0027 v.
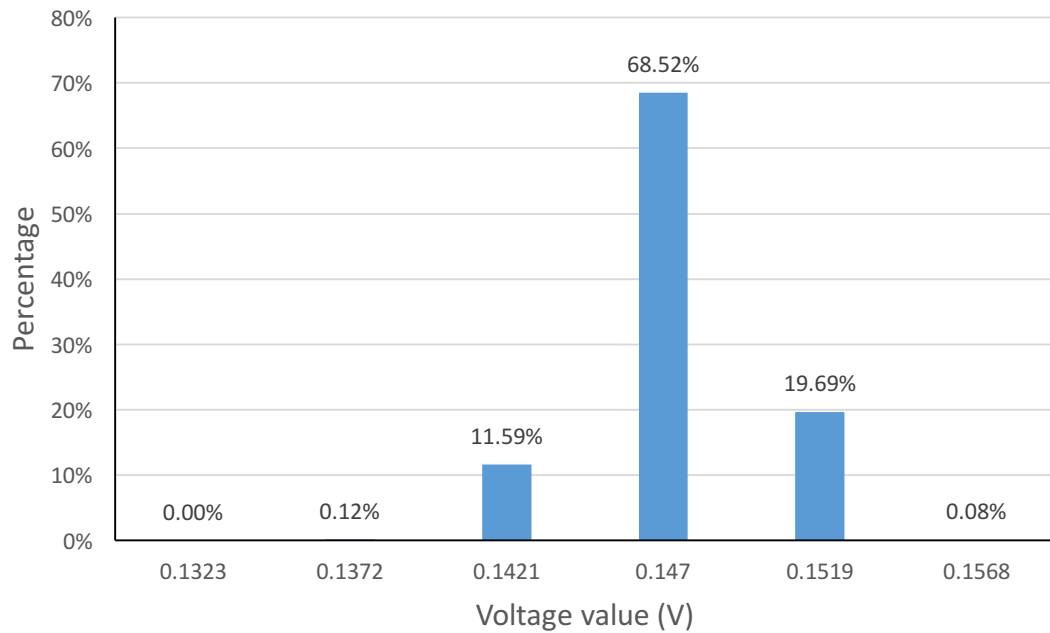
Figure 44. Voltage frenquency data.

As shown in Figure 44, the voltage seen most frequently was 0.147 v (68.52%), and the value fluctuated based on the smallest detectable change (0.0049 v) above and below 0.147 v. The second and third largest quantities were 0.1421 v (0.147-0.0049 v) and 0.1519 v (0.147 +0.0049v), which took up 11.59% and 19.69% of the total readings. The remaining three data points were further away from 0.147 v, and took up less than 0.5% of the total reading.

The other three load cell experimental results had the same graph pattern. Table 4 shows the average voltage, standard deviation, and percent standard deviation for the other three load cells. As described in section 3.1.2, the constant strain and constant force stretching also includes static periods, which was called the rest time. The rest time voltage data from the constant strain and force stretching experiments were collected and are listed in Table 4 for comparison. For all four load cells, the voltage standard deviation, when running the constant force program, was larger than the standard deviation when running the constant strain program where the motor does not move. Comparing the load cell standard deviations, load cell 1 had the smallest standard deviation followed by load cells 2, 4, and 3 respectively. Under the motor off condition, the standard deviations for all four load cells were less than the smallest detectable change. With the constant strain program running, the load cell fluctuates within 2 times of the smallest detectable change. With the constant force program, they fluctuate up to 4 times the smallest detectable change. The reason behind this could be because the motor was on when running the constant strain and force program. When the stepper motor shaft rotates, it vibrates the body frame of the bioreactor and effect the load cell reading.

Table 4. Results for voltage reading when no force change

		Motor off	Constant Strain	Constant Force
Load cell 1	Average voltage	0.0931	0.0835	0.1126
	Standard deviation	0.0015	0.0020	0.0034
	%SD	1.6%	2.4%	3.0%
Load cell 2	Average voltage	0.1329	0.1355	0.1877
	Standard deviation	0.0018	0.0048	0.0083
	%SD	1.4%	3.5%	4.4%
Load cell 3	Average voltage	0.1474	0.1032	0.1201
	Standard deviation	0.0027	0.0120	0.0186
	%SD	1.9%	11.7%	15.5%
Load cell 4	Average voltage	0.1121	0.1029	0.1400
	Standard deviation	0.0020	0.0068	0.0134
	%SD	1.8%	6.6%	9.5%

A second experiment was done with certain displacements. The experiments were performed with different displacements and stretch parameters for all four bioreactor channels, and all the voltage reading results shows a similar pattern. Figure 45 shows one of the test results for channel one. The program was set to run for 3 days, with 1 hour move time and 11 hour rest time. The displacement was set to be 2cm, and the stepper motor shaft rotates with a speed of 8 steps per second with the hold time set to be 3s. Figure 46A shows the voltage change as a function of time. The total number of voltage reading collected by the program was equal to 43,300, and some data points have been deleted following the statistical rule of three. An average of the voltage data was taken for every 200 data points. As we can see, the program was able to perform the desired stretching schedule. Figure 45B shows a closer view of the voltage change during the move time at the beginning of day 2. Voltage was increased during the stretch period and decreased during the release period.
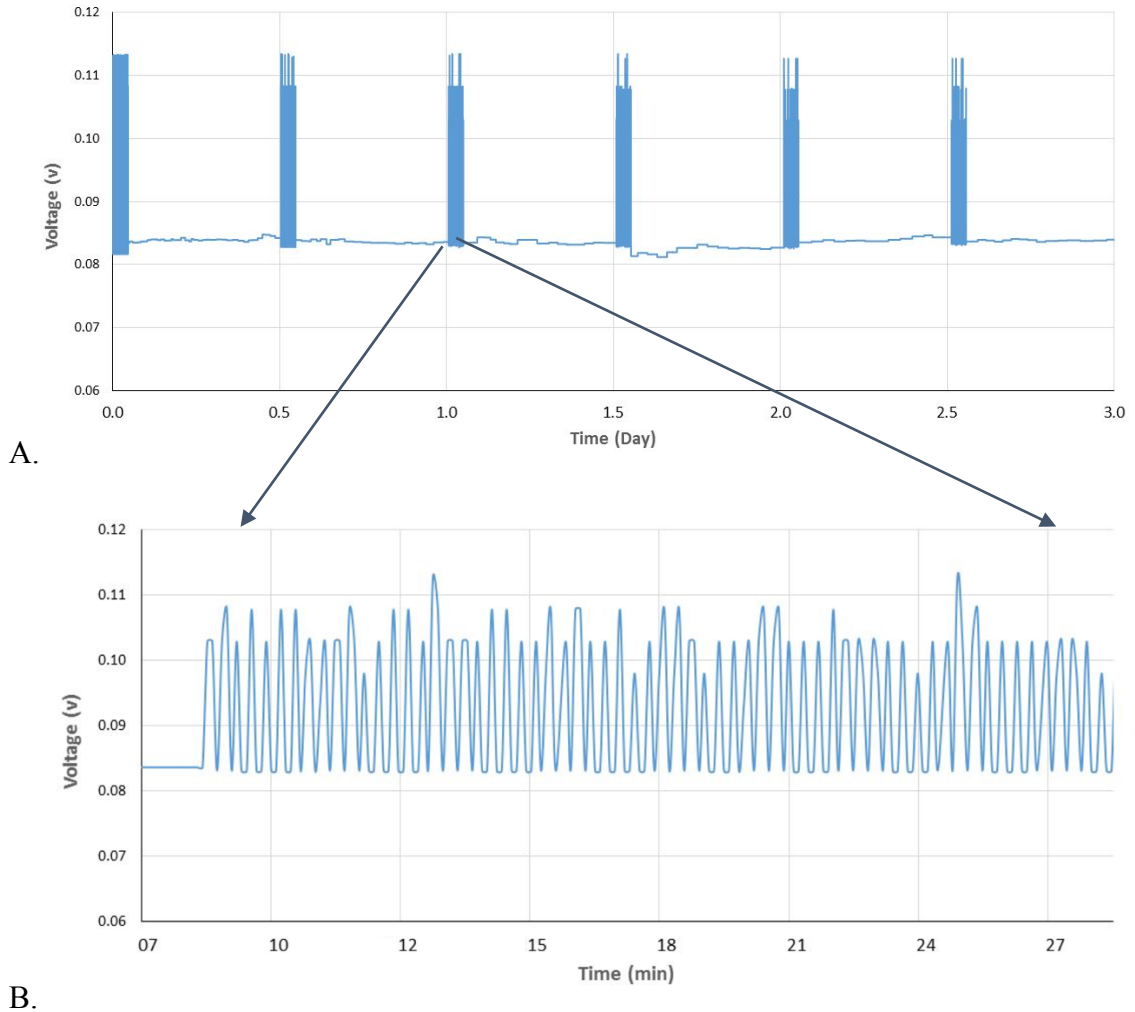
Figure 45. Voltage vs. time graphs from constant strain program.
A. The program set the stepper motor shaft to rotate 2cm back and forth for 1 hour of every 12 hours. Figure 45B shows the voltage data at the move time of day 2. The stretch speed is 8 steps/s and the hole time 1 and 2 were set to be 3s.

3.2.3 Constant Force Program

In order to test the constant force program, test runs were performed with different desired forces values and stretch parameters for all four bioreactor channels. The experimental results show similar graph pattern. Figure 48 shows the voltage vs. time graph of channel one running for three days. Voltage data were processed following the statistical rule of three. The desired force top was 0.6v, and the desired force bottom was 0.2v. The program

was set to run for 3 days, with 1 hour move time and a 5 hour rest time. The total number

of runs is 12, which makes the program run for three days.
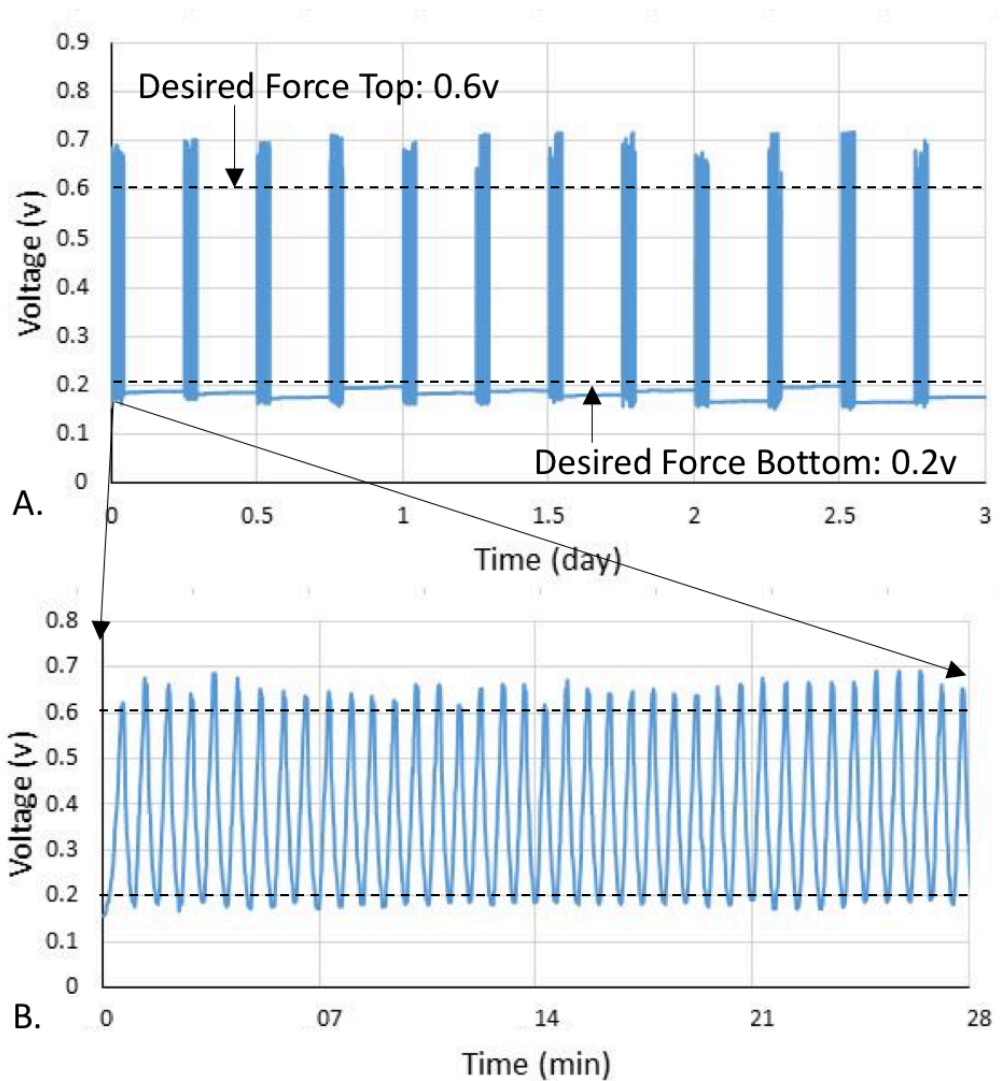
Figure 46. Force vs. time
A. The program set the stepper motor shaft to rotate forward until the voltage reading is 0.6v and rotate backward till the voltage is 0.2v. The program was set to run for 3 days, with 1 hour move time and a 5 hours rest time. Figure 46B shows the closer view voltage change over time at day.

The experimental results show that the programs was able to perform desired stretching

patterns. However, the noise of the voltage data still needs to be reduced. When the

stepper motor is turned off, the voltage data fluctuates $\pm 2 \times 0.0049$v. The ideal condition

when running the strain and force based program would be having a similar accuracy. The load cell sensitivity is high, and the vibration caused by the rotation of the stepper motor shaft affects the load cell reading. The current bioreactor setup has four rods to support the body frame structure, and more rods can be added in the future to help stabilize the load cell and reduce the vibration.

4. VARIABIALITY STUDY OF THE MECHANICAL PROPERTY OF hAMS

The second objective is to study the variability of hAMs mechanical properties. The ideal condition is that the mechanical properties of hAMs is the same at all positions, so that cells attached anywhere to the hAM will experience the same mechanical forces. However, hAMs are a biological material obtained from human placenta, and some intra-donor and inter-donor variance of hAM properties have been reported. It is possible that the mechanical properties vary at different positions of the same hAM sample. When stretching the hAM samples, the thicker part of hAM could be stretched less than the thin part. A standardized processing protocol was used to prepare the hAMs, and the purpose of this study is to find out the degree of variability in the mechanical properties of the processed hAMs.

4.1 Material and Method

4.1.1   hAMs Harvest Process

hAMs were harvested from human placentas. Placentas were collected from the Norman Regional Hospital using protocols that were approved by the Human Subjects Review Boards at both NRH and OU. The hAM was first physically separated from the chorionic membrane of the placenta, and then cut into small pieces (70×110mm). As mentioned in section 1.2.3, the mechanical properties of hAMs varied based on the position. The hAMs were thicker closer to the umbilical cord and thinner on the opposite side near where the membrane breaks prior to birth. When cutting the bulk hAM into small pieces, the part that was within 7cm from the umbilical cord was removed. Additionally, all the membrane pieces were cut so that the pieces were oriented in the same direction. After

obtained the small hAM pieces, a protocol (Figure 47) was followed to decellularize the hAMs. The decellularization procedures included snap freezing at -86°C, detergent treatment (0.03%(w/v) SDS), nuclease treatment (50μg/ml DNase), sterilization (0.2% PAA and 4% Ethanol) and sterile PBS Wash. After the cleaning steps, the membranes were placed in 4°C fridge. It usually took 7 to 10 days to decellularization and produce a batch of membranes (25 to 30) on average.

Snap freezing

↓

Detergent Treatment: 0.03% (w/v) SDS

↓

Nuclease treatment (50μg/ml DNase)

↓

Sterilization: 0.2% PAA and 4% EtOH

↓

Sterile PBS Wash
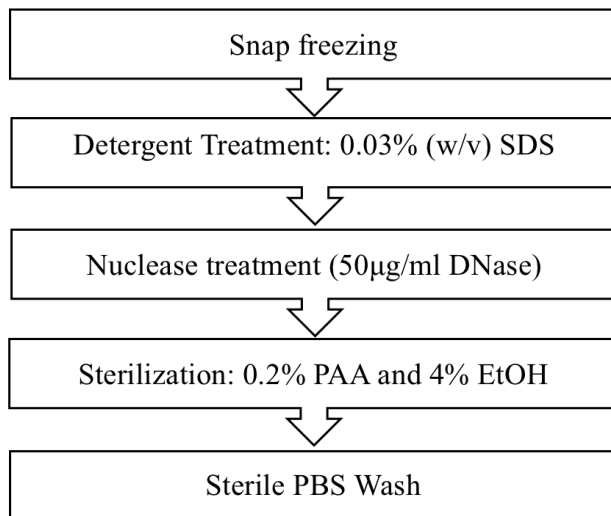
Figure 47. hAM decellularisation protocol

4.1.2 Membrane stretching at different position study

4.1.2.1 Preparation

The hAM sample was marked with at points using blue Sharpie®, show as Figure 48. These points were spaced 15 to 20 mm apart based on the hAM length. These four points separated the membrane into three parts named Top, Middle, and Bottom. The sample was loaded on to the bottom chamber only, and the bottom chamber was modified by cutting the front wall off for a better view. A ruler was placed next to the hAM to measure the position. Figure 48 also includes a zoomed in reading view, which shows that the

position can be clearly read. PBS was sprayed onto the membrane to keep the sample hydrated.
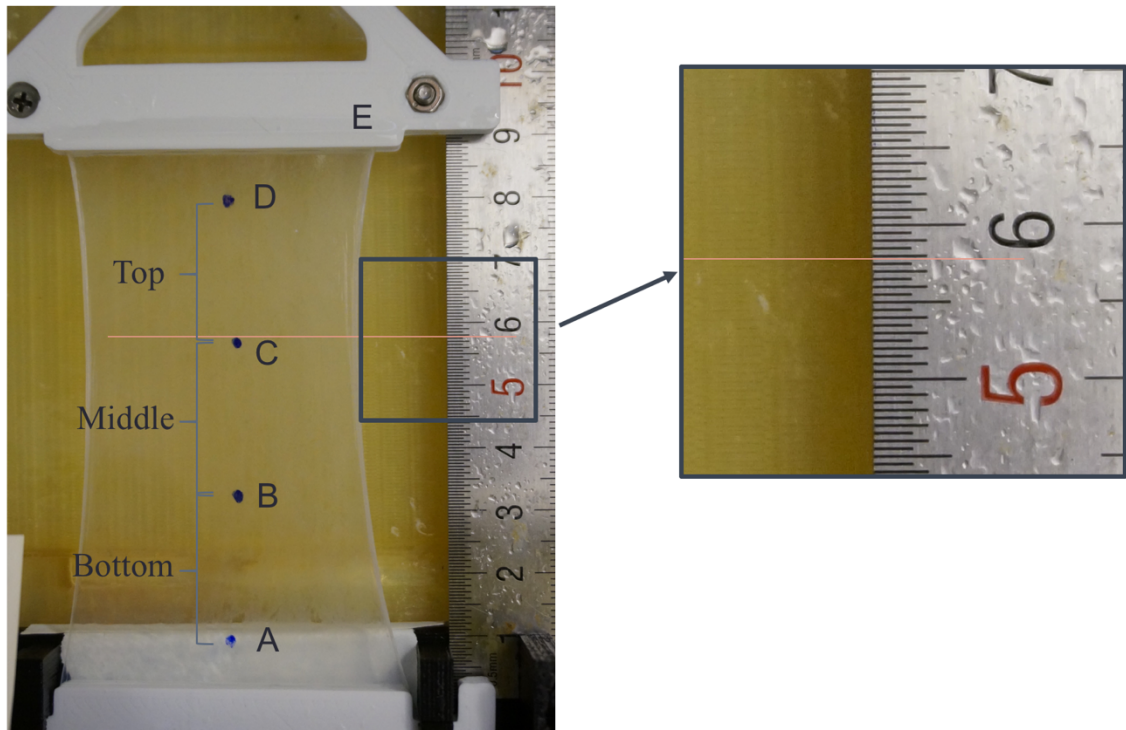
Figure 48. Example of position reading on the hAM sample.

4.1.2.2 Experimental procedure

Pre-stretch program, described in section 3.1.1, was used to adjust the sample to the 0% strain position, where the sample was at its original length. A picture was taken to record the original positions of A, B, C, D and E. The membrane sample was then stretched to a certain percent strain using the strain based stretching program. Another picture was taken to record the new position. It was important to make sure the sample was at 0% strain position again before the new percent strain test. Repeat the steps for another percent strain test.

4.1.2.3 Data Reading and Processing

Place the picture taken before and after stretching into power point, and then add a horizontal line onto the picture to help read the position of each point as shown in Figure 48. The reading at point A, B, C, D, and E for both before and after stretching were recorded as shown in Figure 49A. The distance between point A and B was defined as the Bottom distance, the distance between B and C was called the Middle distance, and the distance between C and D was called the Top distance. The length of Top, Middle and Bottom distance before and after stretching were calculated with an excel table as Figure 49B with an example. The equations used for the calculations are shown in Figure 49C with the Bottom distance as an example. Measured strain was the difference divided by the sample length before stretching, and normalized strain was the measured strain divided by the applied strain.

% strain (actual)	Bottom to top				
2.30%	A	B	C	D	E
Before	0.8	3.35	5.9	8.1	8.9
After	0.81	3.44	6.04	8.29	9.1

A

	Bottom	Middle	Top
length before	2.55	2.55	2.2
length after	2.63	2.6	2.25
Difference	0.080	0.050	0.050
Measured strain	3%	2%	2%
Normalized strain	136%	85%	99%

B

	Bottom
length before	b-a
length after	b'-a'
Difference	(b'-a')-(b-a)
Measured strain	Difference/length before
Normalized strain	Measured strain/applied strain

C

Figure 49 Example of data processing.

The error of the normalized strain was also calculated with a formula below. The position of all points were read by human eyes, and there is a reading error of 0.1mm. The derivation of the formula is shown in Appendix A. The error of normalized strain was higher at low strain stretching than high strain.

$$du = \sqrt{2\left(\frac{X+sY}{X^2}\right)^2 (Sa)^2 + 2\left(\frac{1}{X}\right)^2 (Sa)^2 + \left(\frac{(a-b)Y}{X^2}\right)^2 (Ss)^2}$$

Four groups of experiments have been done for this study. The first group was done with single layer hAMs (n=20). The second group was with two layer of hAMs (n=5). The third group was with two layer hAMs attached with fibrin glue (n=4). The fourth group was two-layer hAMs attached by surgical glue named GLUture Topical Tissue Adhesive (32046, World Precision Instruments, Florida, USA) (n=3). Each hAM sample were stretched to different strain, divided into groups of 1 to 1.5% strain, 1.5 to 2% strain, 2 to 3% strain, and 3 to 4% strain. A close to 100% normalized strain result means that the part of membrane has been stretched to the desired strain. If the normalized strain values were different at different positions, it meant the mechanical property of the processed hAM were not consistent. Variance of the data points were also studied. Variance indicates how close each data set was to the average value. The smaller the variance value was, the closer to the average normalized strain, which indicate that the hAMs stretching character more consistent.

4.2 Result and discussion

4.2.1 hAMs stretching at different position study

Figure 50 shows the normalized strain at three different positions (Top, Middle and Bottom) for single layer hAM as a function of applied strain. hAM samples were used in this experiment, and the error bar shows the standard error of the mean. The data shows that there was no significant difference in normalized strain between the Bottom, Middle, and Top part of the hAM (P>0.05). Additionally, there was also no significant difference between 1 to 1.5%, 1.5-2%, and 2%-3% strain stretching (t-test, p>0.05). However, the variance value (shown as figure 51) for 3-4% stretching was a lot lower than the 1-1.5%

74

and 1.5-2% (P<0.05). The normalized strain result indicates that there was no difference in hAM mechanical properties between different positions or different applied strains. The variance result indicates that one layer hAMs stretch consistently at different positions with higher strain.
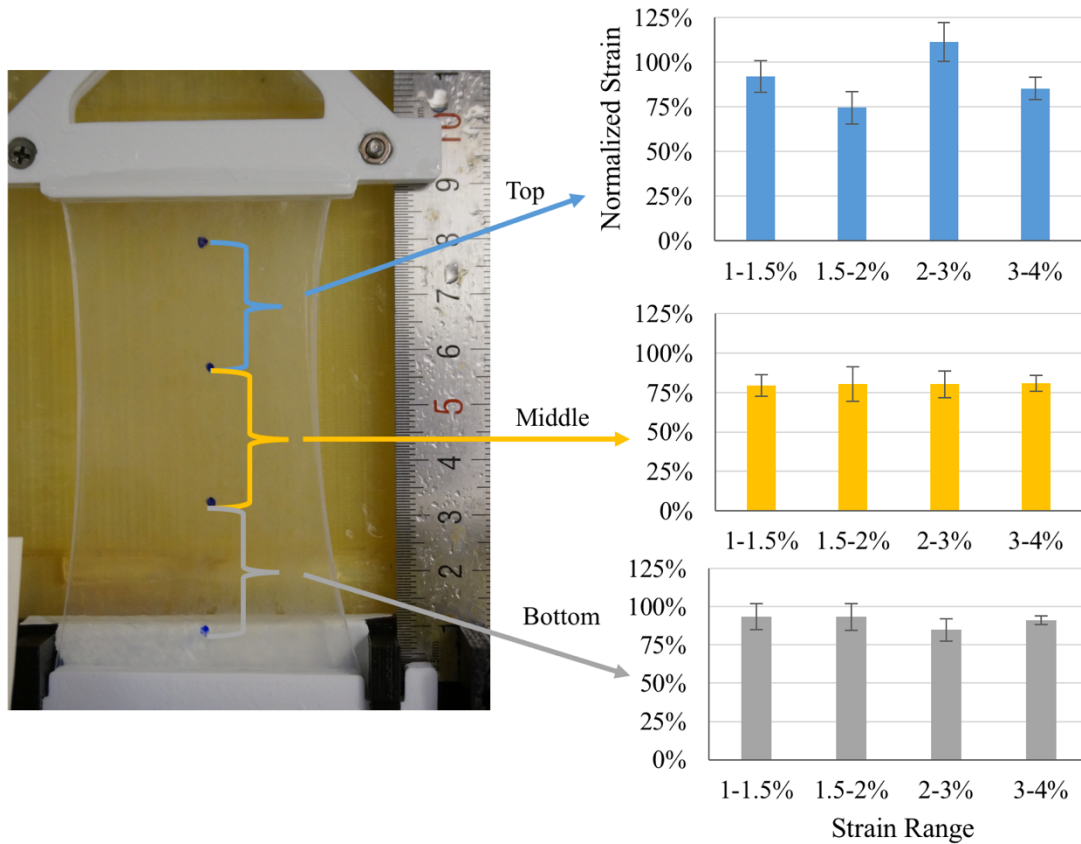
Figure 50. Normalized strain at three different positions for single layer hAM as a function of applied strain. Error bars show s.e.m. for n=20. t-test results show that none of the resutls are significantly different from one another.
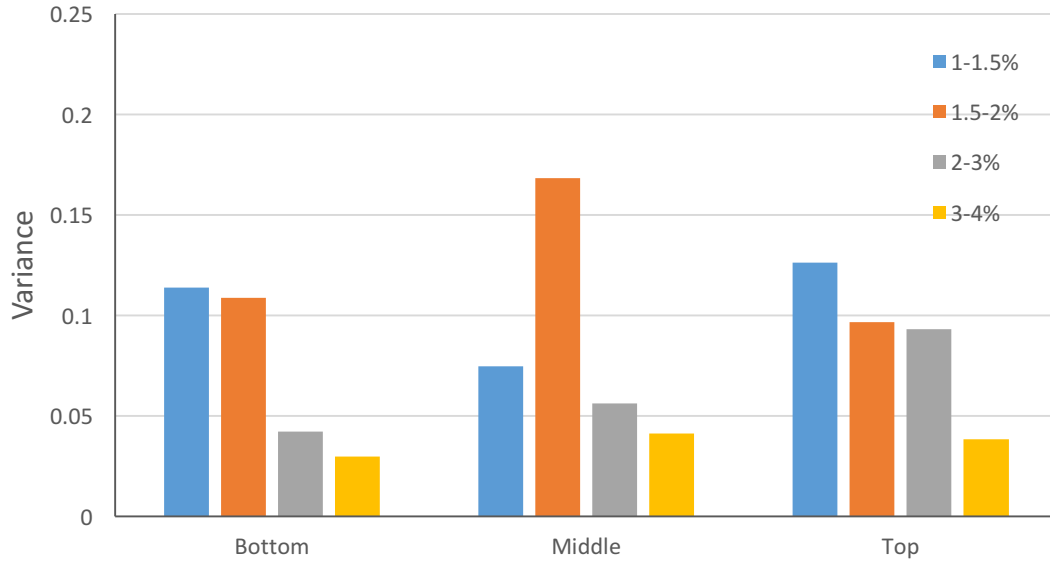
Figure 51. Variance at different positions for single layer hAM as a function of applied strain. for n=20. t-test results show that 1-1.5% is differernt from 3-4% strain.

Figure 52 shows the normalized strain at the three different positions for the two-layer hAM as a function of applied strain. The result shows that the normalized strain value does not significantly differ at the three positions with all four strain groups. The variance value (shown as figure 53) for 3-4% stretching was a lot lower than the low strain 1-1.5% groups. (p<0.05).

The experiment results for the two layer hAMs are very similar to the one-layer hAM. They all indicate that there is no significant mechanical property difference between the top, middle and bottom part of the hAMs (55×75mm).

Figure 52. Normalized strain at three different positions for two layer hAM as a function of applied strain. Error bars show s.e.m. for n=5. t-test results show that none of the results are significantly different from one another.
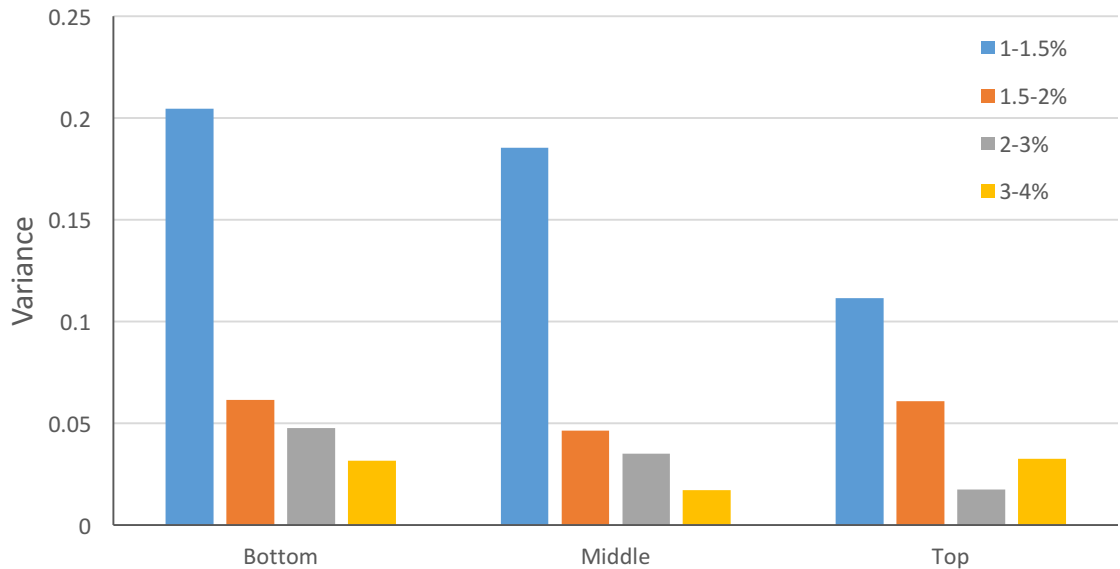
Figure 53. Variance at different positions for two layer hAM as a function of applied strain. for n=5. t-test results show that 1-1.5% is differernt from 3-4% strain.

Figure 54 shows the normalized strain at the three different positions for the two-layer hAM attached by fibrin glue as a function of applied strain. Fibrin glue was applied in between the hAMs. The result shows no significant different between three different positions with all four applied strains. However, the variance data, as shown in Figure 55,

is a lot larger compare to the one and two layer hAMs experiment. The variance value of

the first two experiment are within 0.2, but the highest variance value is 0.43 in this group.

Figure 54. Normalized strain at three different positions for two layer hAM with fibrin glue as a function of applied strain. Error bars show s.e.m. for n=4. t-test results show that none of the results are significantly different from one another.
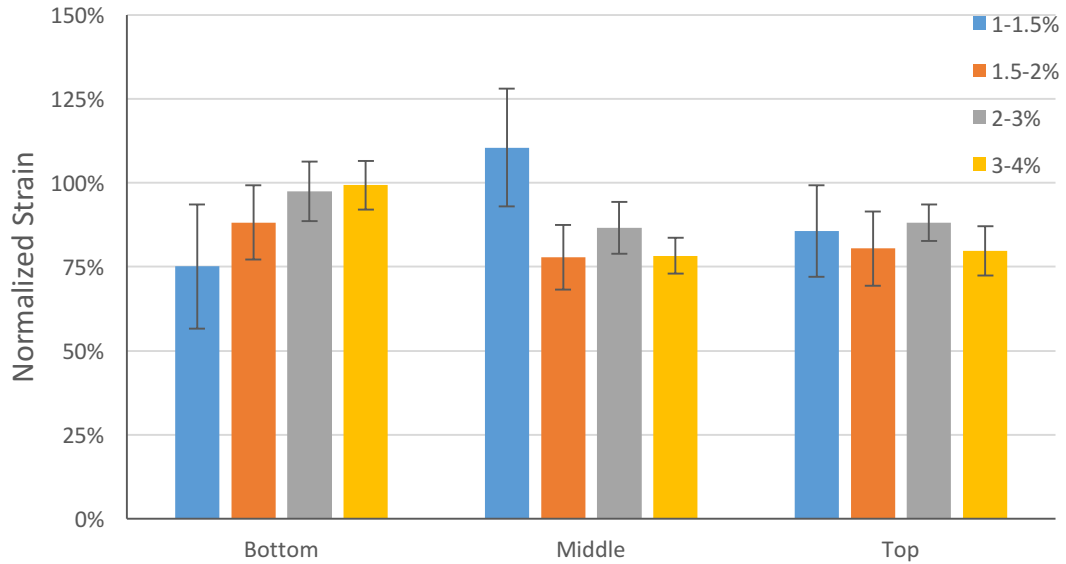

Figure 55. Variance at different positions for two layer hAM attatched by fibrin glue as a function of applied strain. for n=4. t-test results show that none of the results are significantly different from one another.

Normalized strain experiments were also performed with the two layer membranes

attached by surgical glue called GLUture Topical Tissue Adhesive (32046, World

Precision Instruments, Florida, USA). After applying GLUture between two layers of hAM, the samples become more stiff compared to the samples without glue. Figure 56 shows the Young's modulus data of different tissue samples. The t-test result suggests that there is no significant difference between one layer, two layer and two layer with fibrin glue. (p>0.05). However, the Young's modulus value of two layer with surgical glue is higher than the one-layer hAM. (p<0.05)
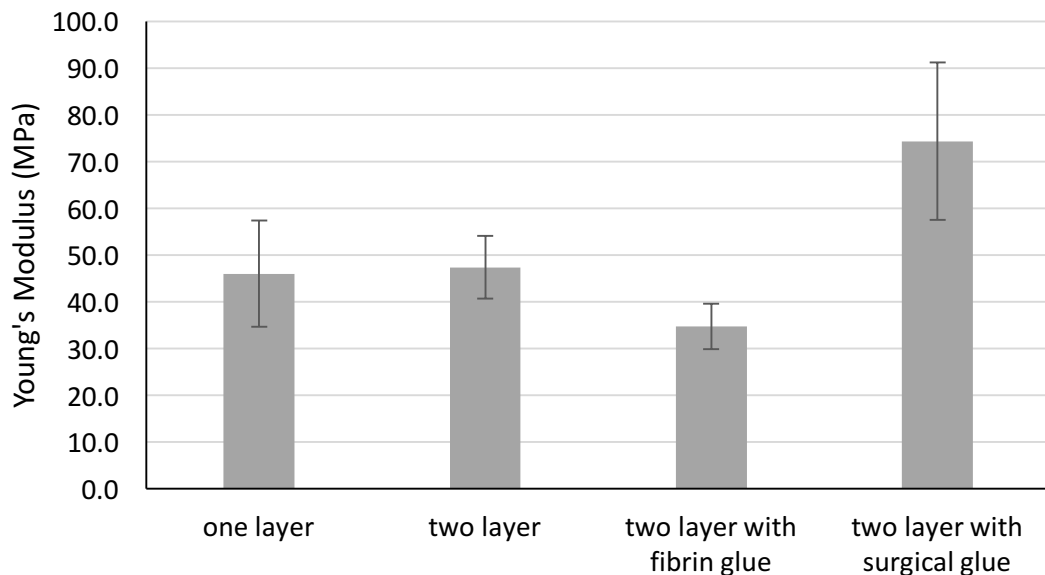
Figure 56. Young's modulus of the four different tissue samples. Error bars show s.e.m.
The t-test result shows that there is no significant difference between one layer, two layer and two layer with fibrin glue (p>0.05). The two-layer hAM with surgical glue result is different than the one-layer hAM. (p<0.05) n=15 for one layer, n=3 for two layer, two layer with fibrin glue, and two layer with surgical glue.

Figure 57 and 58 are the experimental results for GLUture tissue samples. During the stretching process, the glue starts to break into smaller pieces. Thus the GLUture experiment was only repeated three times as a reference.
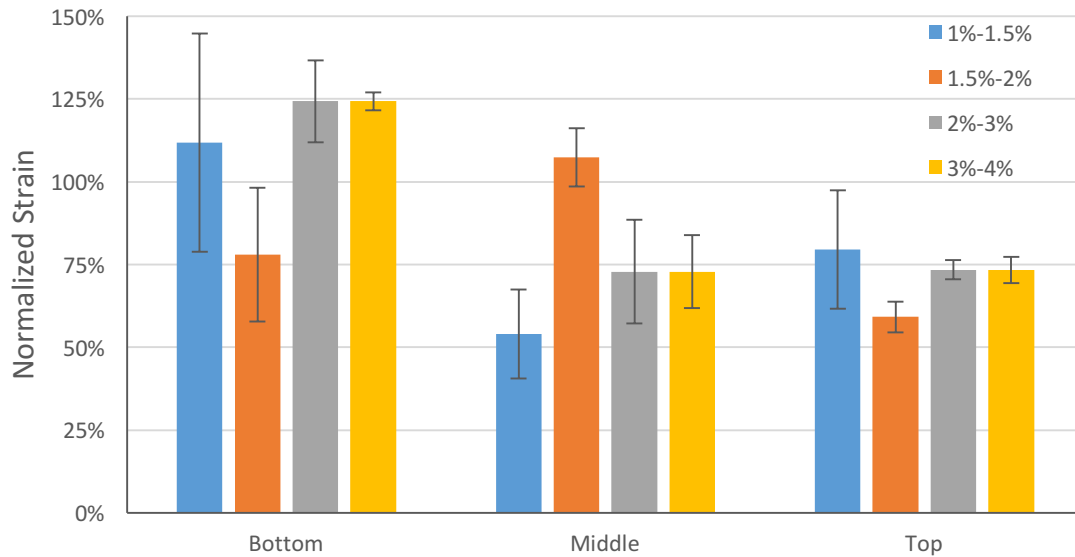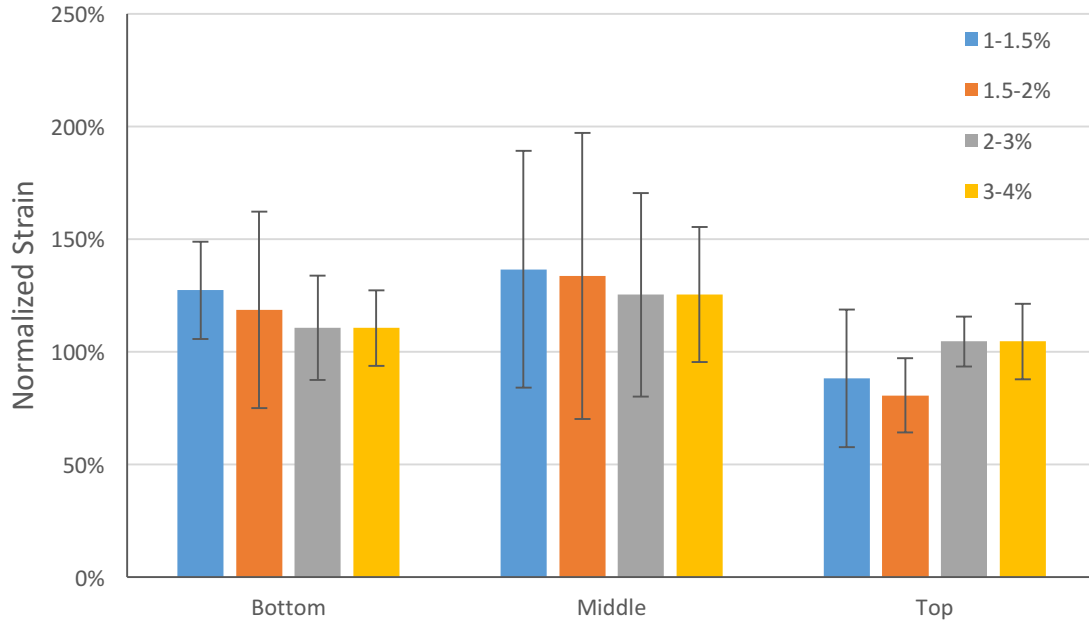
Figure 57. Normalized strain at three different positions for two layer hAM with surgical glue as a function of applied strain. Error bars show s.e.m. for n=3. t-test results show that none of the results are significantly different from one another.
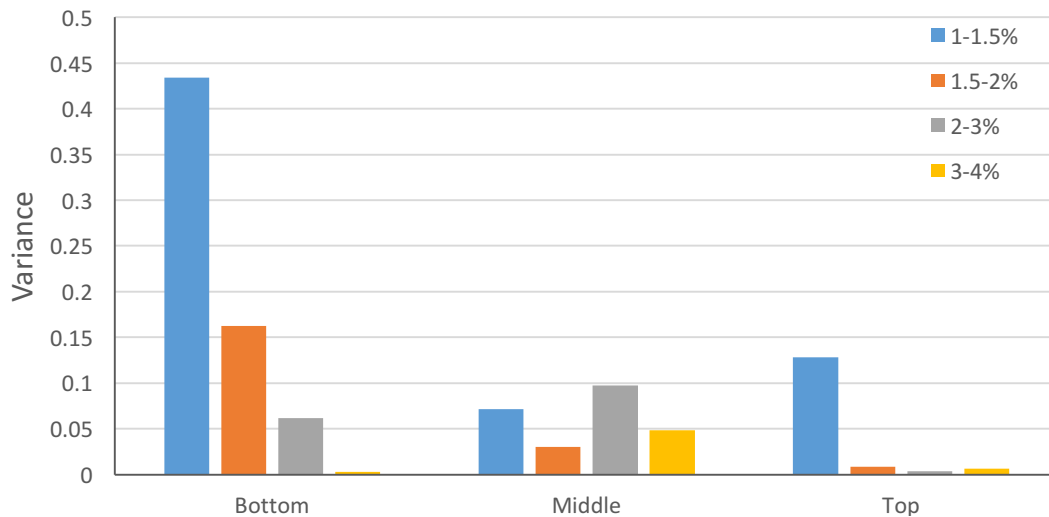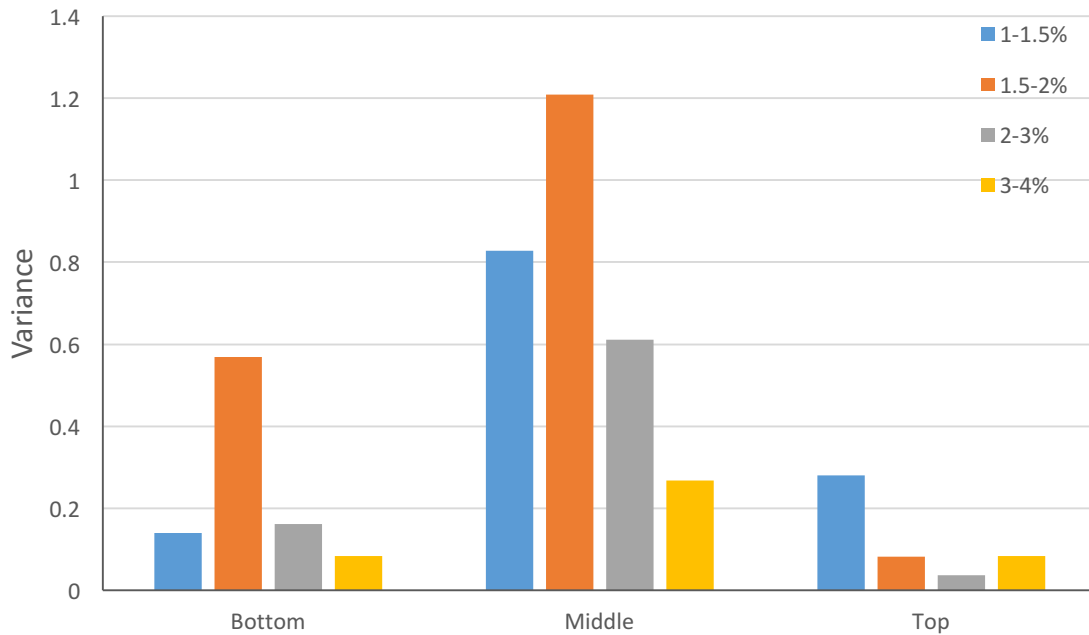

Figure 58. Variance at different positions for two layer hAM attatched by sugical glue as a function of applied strain. for n=4. t-test resuts show that none of the results are significantly different from one another.

From the above experimental results, it comes to conclusion that there is no significate mechanical property difference between the top, middle and bottom part of the hAMs. It also shows that when stretch the hAM with 1-1.5% strain, it has a higher variance value compare to than 3-4% strain. The means the stretching character is more consistent at 3-4% strain. The variance value is higher when the tissue sample was attached with glue, this is because the tissue mechanical structure becomes more complex. All the experiments were performed with the tissue sample width between 50 to 55mm, and length between 70 to 80 mm, so the results apply only to these specific dimensions used in this study.

5. CONCLUSION AND FUTURE DIRECTION

A tendon tissue engineering bioreactor system, providing a tissue culture environment and mechanical stimulation, has been designed in this study. Stepper motors, load cells, and Arduino boards were used to provide mechanical stimulation and monitor the force changes. Three programs, written with LabVIEW, made it possible for this bioreactor to have tunable and cyclic stretching parameters. The pre-stretch program was developed to adjust the tissue sample to any required initial position. The strain based stretching program was used to provide cyclic mechanical stimulations with a constant strain and monitor the force change. The force based stretching program provided a constant force based mechanical stimulation to the tissue sample. With these three programs, the tissue sample was adjusted to a known initial position and then stretched with a constant force, which corresponded to a certain strain. The current bioreactor setup has four rods to support the body frame structure, and more rods can be added in the future to help stabilize the load cell and reduce the vibration.

This bioreactor system also has the potential to compare the mechanical properties of the same tissue sample at different times during the culturing period. This can be accomplished by recording the force corresponding to 0%, 1%, and 2% strain, and compare the force change. The larger the force needed to reach the same strain, the stronger the material has become. This study should be continued in the future to analyze how the mechanical properties of the tissue sample change with time.

The variability of the mechanical property of the hAMs was also studied with the use of the strain based stretching program. The experimental results indicate that the decellularized hAMs have consistent mechanical properties at the three different

positions. The variance value was compared between different applied strains, and it suggested that the high strain 3-4% have lower variance than 1-1.5% strain (p<0.05). The percent difference study on the displacement adjustment curve discussed in section 2.2.2 suggested that the curve is more precise when the applied displacement is larger than 1mm. Based on the result of these two studies, we suggest that a 1.5% should be added to the tissues as the initial position before adding mechanical stimulation.

Reference

1.   Oh, L.S., et al., *Indications for rotator cuff repair: a systematic review.* Clin Orthop Relat Res, 2007. **455**: p. 52-63.

2.   Paxton, E.S., et al., *Clinical and radiographic outcomes of failed repairs of large or massive rotator cuff tears: minimum ten-year follow-up.* J Bone Joint Surg Am, 2013. **95**(7): p. 627-32.

3.   Yan, Z., et al., *Boosting tendon repair: interplay of cells, growth factors and scaffold-free and gel-based carriers.* J Exp Orthop, 2018. **5**(1): p. 1.

4.   *Rotator cuff* 2018.

5.   *Rotator Cuff Injury.* 2018, Mayo Clinic.

6.   Doral, M.N., et al., *Functional anatomy of the Achilles tendon.* Knee Surg Sports Traumatol Arthrosc, 2010. **18**(5): p. 638-43.

7.   Wang, J.H., *Mechanobiology of tendon.* J Biomech, 2006. **39**(9): p. 1563-82.

8.   Riley, G.P., et al., *Glycosaminoglycans of human rotator cuff tendons: changes with age and in chronic rotator cuff tendinitis.* Ann Rheum Dis, 1994. **53**(6): p. 367-76.

9.   Thorpe, C.T., et al., *The role of the non-collagenous matrix in tendon function.* Int J Exp Pathol, 2013. **94**(4): p. 248-59.

10.   Gomes, M.E., R.L. Reis, and M.r. Rodrigues, *Tendon regeneration : understanding tissue physiology and development to engineer functional substitutes.* 2015: London : Elsevier.

11.   Lin, J.C., N. Weintraub, and D.R. Aragaki, *Nonsurgical Treatment for Rotator Cuff Injury in the Elderly.* Journal of the American Medical Directors Association, 2008. **9**(9): p. 626-632.

12.   Edward, T.S., et al., *The Use of Electrospun Scaffolds in Musculoskeletal Tissue Engineering: A Focus on Tendon.* Current Stem Cell Research & Therapy, 2018. **13**: p. 1-13.

13.   Yamamoto, A., et al., *Prevalence and risk factors of a rotator cuff tear in the general population.* J Shoulder Elbow Surg, 2010. **19**(1): p. 116-20.

14.   Praemer, A., S. Furner, and D. P. Rice, *Musculoskeletal conditions in the United States / Allan Praemer, Sylvia Furner, Dorothy P. Rice.* 2018.

15.   Beldjilali-Labro, M., et al., *Biomaterials in Tendon and Skeletal Muscle Tissue Engineering: Current Trends and Challenges.* Materials (Basel), 2018. **11**(7).

16.   Sultana, N., *Biodegradable polymer-based scaffolds for bone tissue engineering.* 2013, Springer: Berlin ;.

17.   Prabhath, A., et al., *Growth factor delivery strategies for rotator cuff repair and regeneration.* Int J Pharm, 2018. **544**(2): p. 358-371.

18.   Barber, F.A., M.A. Herbert, and M.H. Boothby, *Ultimate tensile failure loads of a human dermal allograft rotator cuff augmentation.* Arthroscopy, 2008. **24**(1): p. 20-4.

19.   Docheva, D., et al., *Biologics for tendon repair.* Adv Drug Deliv Rev, 2015. **84**: p. 222-39.

20.   Chaudhury, S., et al., *Tensile and shear mechanical properties of rotator cuff repair patches.* J Shoulder Elbow Surg, 2012. **21**(9): p. 1168-76.

21.   Itoi, E., et al., *Tensile properties of the supraspinatus tendon.* J Orthop Res, 1995. **13**(4): p. 578-84.

22.   Derwin, K., et al., *Rotator cuff repair: challenges and solutions.* Orthopedic Research and Reviews, 2015.

23.   Wu, X.L., L. Briggs, and G.A. Murrell, *Intraoperative determinants of rotator cuff repair integrity: an analysis of 500 consecutive repairs.* Am J Sports Med, 2012. **40**(12): p. 2771-6.

24.   Ratcliffe, A., et al., *Scaffolds for tendon and ligament repair and regeneration.* Ann Biomed Eng, 2015. **43**(3): p. 819-31.

25.   Shi, Y. and I. Vesely, *A dynamic straining bioreactor for collagen-based tissue engineering*, in *Bioreactors for Tissue Engineering.* 2005, Springer. p. 209-219.

26.   Bi, Y., et al., *Identification of tendon stem/progenitor cells and the role of the extracellular matrix in their niche.* Nat Med, 2007. **13**(10): p. 1219-27.

27.   Chen, J., et al., *Characterization and comparison of post-natal rat Achilles tendon-derived stem cells at different development stages.* Sci Rep, 2016. **6**: p. 22946.

28.   Stegemann, J.P., H. Hong, and R.M. Nerem, *Mechanical, biochemical, and extracellular matrix effects on vascular smooth muscle cell phenotype.* J Appl Physiol (1985), 2005. **98**(6): p. 2321-7.

29.   Derwin, K.A., et al., *Commercial extracellular matrix scaffolds for rotator cuff tendon repair. Biomechanical, biochemical, and cellular properties.* J Bone Joint Surg Am, 2006. **88**(12): p. 2665-72.

30.   Ricchetti, E.T., et al., *Scaffold devices for rotator cuff repair.* J Shoulder Elbow Surg, 2012. **21**(2): p. 251-65.

31.   Aamodt, J.M. and D.W. Grainger, *Extracellular matrix-based biomaterial scaffolds and the host response.* Biomaterials, 2016. **86**: p. 68-82.

32.   Wang, T., et al., *Bioreactor design for tendon/ligament engineering.* Tissue Eng Part B Rev, 2013. **19**(2): p. 133-46.

33.   Drury, J.L. and D.J. Mooney, *Hydrogels for tissue engineering: scaffold design variables and applications.* Biomaterials, 2003. **24**(24): p. 4337-4351.

34.   Niknejad, H., et al., *Properties of the amniotic membrane for potential use in tissue engineering.* Eur Cell Mater, 2008. **15**: p. 88-99.

35.   Dua, H.S., et al., *Variations in amniotic membrane: relevance for clinical applications.* Br J Ophthalmol, 2010. **94**(8): p. 963-4.

36.   Lopez-Valladares, M.J., et al., *Donor age and gestational age influence on growth factor levels in human amniotic membrane.* Acta Ophthalmol, 2010. **88**(6): p. e211-6.

37.   Connon, C.J., et al., *The variation in transparency of amniotic membrane used in ocular surface regeneration.* Br J Ophthalmol, 2010. **94**(8): p. 1057-61.

38.   Niknejad, H., et al., *The effects of preservation procedures on amniotic membrane's ability to serve as a substrate for cultivation of endothelial cells.* Cryobiology, 2011. **63**(3): p. 145-51.

39.   Arrizabalaga, J.H. and M.U. Nollert, *Human Amniotic Membrane: A Versatile Scaffold for Tissue Engineering.* ACS Biomaterials Science & Engineering, 2018.

40.   Wolbank, S., et al., *Impact of human amniotic membrane preparation on release of angiogenic factors.* J Tissue Eng Regen Med, 2009. **3**(8): p. 651-4.

41.   Sharma, P. and N. Maffulli, *Biology of tendon injury: healing, modeling and remodeling.* J Musculoskelet Neuronal Interact, 2006. **6**(2): p. 181-90.

42.   contributors, P., *Bibliographic details for Tendon Biomechanics.* 2017, Physiopedia.

43.   Joshi, S.D. and K. Webb, *Variation of cyclic strain parameters regulates development of elastic modulus in fibroblast/substrate constructs.* J Orthop Res, 2008. **26**(8): p. 1105-13.

44.   Saber, S., et al., *Flexor tendon tissue engineering: bioreactor cyclic strain increases construct strength.* Tissue Eng Part A, 2010. **16**(6): p. 2085-90.

45.   Woon, C.Y., et al., *Three-dimensional-construct bioreactor conditioning in human tendon tissue engineering.* Tissue Eng Part A, 2011. **17**(19-20): p. 2561-72.

46.   Altman, G.H., et al., *Advanced bioreactor with controlled application of multi-dimensional strain for tissue engineering.* J Biomech Eng, 2002. **124**(6): p. 742-9.

47.   Juncosa-Melvin, N., et al., *Effects of mechanical stimulation on the biomechanics and histology of stem cell-collagen sponge constructs for rabbit patellar tendon repair.* Tissue Eng, 2006. **12**(8): p. 2291-300.

48.   Webb, K., et al., *Cyclic strain increases fibroblast proliferation, matrix accumulation, and elastic modulus of fibroblast-seeded polyurethane constructs.* J Biomech, 2006. **39**(6): p. 1136-44.

49.   Androjna, C., R.K. Spragg, and K.A. Derwin, *Mechanical conditioning of cell-seeded small intestine submucosa: a potential tissue-engineering strategy for tendon repair.* Tissue Eng, 2007. **13**(2): p. 233-43.

50.   Nirmalanandhan, V.S., et al., *Improving linear stiffness of the cell-seeded collagen sponge constructs by varying the components of the mechanical stimulus.* Tissue Eng Part A, 2008. **14**(11): p. 1883-91.

51.   Nguyen, T.D., et al., *Effects of cell seeding and cyclic stretch on the fiber remodeling in an extracellular matrix-derived bioscaffold.* Tissue Eng Part A, 2009. **15**(4): p. 957-63.

52.   Abousleiman, R.I., et al., *Tendon tissue engineering using cell-seeded umbilical veins cultured in a mechanical stimulator.* Tissue Eng Part A, 2009. **15**(4): p. 787-95.

53.   Butler, D.L., et al., *Using functional tissue engineering and bioreactors to mechanically stimulate tissue-engineered constructs.* Tissue Eng Part A, 2009. **15**(4): p. 741-9.

54.   Chen, J.L., et al., *Efficacy of hESC-MSCs in knitted silk-collagen scaffold for tendon tissue engineering and their roles.* Biomaterials, 2010. **31**(36): p. 9438-51.

55.   Bilgen, B., et al., *Design of a biaxial mechanical loading bioreactor for tissue engineering.* J Vis Exp, 2013(74): p. e50387.

56.   Wang, T., et al., *Programmable mechanical stimulation influences tendon homeostasis in a bioreactor system.* Biotechnol Bioeng, 2013. **110**(5): p. 1495-507.

57. Laurent, C., et al., *Towards a Tissue-Engineered Ligament: Design and Preliminary Evaluation of a Dedicated Multi-Chamber Tension-Torsion Bioreactor.* Processes, 2014. **2**(1): p. 167-179.

58. Goodhart, J., et al., *Design and Validation of a Cyclic Strain Bioreactor to Condition Spatially-Selective Scaffolds in Dual Strain Regimes.* Processes, 2014. **2**(2): p. 345-360.

59. Youngstrom, D.W., et al., *A bioreactor system for in vitro tendon differentiation and tendon tissue engineering.* J Orthop Res, 2015. **33**(6): p. 911-8.

60. Qin, T.W., et al., *Effect of mechanical stimulation on bone marrow stromal cell-seeded tendon slice constructs: a potential engineered tendon patch for rotator cuff repair.* Biomaterials, 2015. **51**: p. 43-50.

61. Cook, C.A., et al., *Characterization of a novel bioreactor system for 3D cellular mechanobiology studies.* Biotechnol Bioeng, 2016. **113**(8): p. 1825-37.

62. Wu, S., et al., *Living nanofiber yarn-based woven biotextiles for tendon tissue engineering using cell tri-culture and mechanical stimulation.* Acta Biomater, 2017. **62**: p. 102-115.

63. *LigaGen: Tension Bioreactor System*. 2018 [cited 2018 April]; Available from: http://www.tissuegrowth.com/prod_ligament.cfm.

64. Parent, G., N. Huppe, and E. Langelier, *Low stress tendon fatigue is a relatively rapid process in the context of overuse injuries.* Ann Biomed Eng, 2011. **39**(5): p. 1535-45.

65. Engebretson, B., Z.R. Mussett, and V.I. Sikavitsas, *The effects of varying frequency and duration of mechanical stimulation on a tissue-engineered tendon construct.* Connect Tissue Res, 2018. **59**(2): p. 167-177.

66. Wells, L.K. and J. Travis, *LabVIEW for everyone : graphical programming made even easier*. 1997, Upper Saddle River, NJ: Prentice Hall PTR.

Appendix

Reading error calculation

	Point A	Point B	Point E
Reading before stretching	a	b	e
Reading after stretching	a'	b'	e'

Applied strain (s): (e'-e)/sample length

Length before stretching: b-a

Length after stretching: b'-a'

Difference= (b'-a')-(b-a)

$$\text{Measured strain} = \frac{(b' - a') - (b - a)}{b - a}$$

$$\text{Normalized strain} = \frac{Measured\ strain}{Applied\ strain} = \frac{(b' - a') - (b - a)}{(b - a) \times s}$$

$$\%\ \text{accomplished} = U = \frac{(b' - a') - (b - a)}{(b - a) \times s} = \frac{Y}{X}$$

$$Y = (b' - a') - (b - a)$$

$$X = (b - a) \times s$$

$$du^2 = \left(\frac{du}{da}\right)^2 (Sa)^2 + \left(\frac{du}{da'}\right)^2 (Sa')^2 + \left(\frac{du}{db}\right)^2 (Sb)^2 + \left(\frac{du}{db'}\right)^2 (Sb)^2 + \left(\frac{du}{ds}\right)^2 (Ss)^2$$

$$\frac{du}{da} = \frac{X + sY}{X^2}$$

$$\frac{du}{da'} = \frac{-1}{X}$$

$$\frac{du}{db} = \frac{-X - sY}{X^2}$$

$$\frac{du}{db'} = \frac{1}{X}$$

$$\frac{du}{ds} = \frac{(a - b)Y}{X^2}$$

$$du^2 = \left(\frac{X+sY}{X^2}\right)^2 (Sa)^2 + \left(\frac{-1}{X}\right)^2 (Sa')^2 + \left(\frac{-X-sY}{X^2}\right)^2 (Sb)^2 + \left(\frac{1}{X}\right)^2 (Sb)^2 +$$

$$\left(\frac{(a-b)Y}{X^2}\right)^2 (Ss)^2$$

$$Sa = Sa' = Sb = Sb' = Se = Se'$$

$$du^2 = 2\left(\frac{X + sY}{X^2}\right)^2 (Sa)^2 + 2\left(\frac{1}{X}\right)^2 (Sa)^2 + \left(\frac{(a-b)Y}{X^2}\right)^2 (Ss)^2$$

$$du = \sqrt{2\left(\frac{X + sY}{X^2}\right)^2 (Sa)^2 + 2\left(\frac{1}{X}\right)^2 (Sa)^2 + \left(\frac{(a-b)Y}{X^2}\right)^2 (Ss)^2}$$

$$\text{Applied} = s = \frac{e' - e}{Sample\ length(L)}$$

$$S_s = \frac{1}{L^2}Se^2 + \frac{1}{L^2}Se'^2 = \frac{2}{L^2}Sa^2$$

$$du = \sqrt{2\left(\frac{X+sY}{X^2}\right)^2 (Sa)^2 + 2\left(\frac{1}{X}\right)^2 (Sa)^2 + 2\left(\frac{(a-b)Y}{X^2 L}\right)^2 (Sa)^2}$$